Synthesis of reactive phosphorus-based carbonate for flame retardant polyhydroxyurethane foams

Guilhem Coste, Maxinne Denis, Rodolphe Sonnier, Sylvain Caillol, Claire Negrell-Guirao

Synthesis of reactive phosphorus-based carbonate for flame retardant polyhydroxyurethane foams

Guilhem Coste[a], Maxinne Denis[a], Rodolphe Sonnier[b], Sylvain Caillol[a]*, Claire Negrell[a*]

[a] *ICGM, Univ Montpellier, CNRS, ENSCM, Montpellier, France*
[b]

Polymers Composites and Hybrids (PCH), IMT Mines Ales, Ales, France
**Corresponding author: Claire Negrell, email: claire.negrell@enscm.fr; Sylvain Caillol, email: sylvain.caillol@enscm.fr*

Graphical abstract

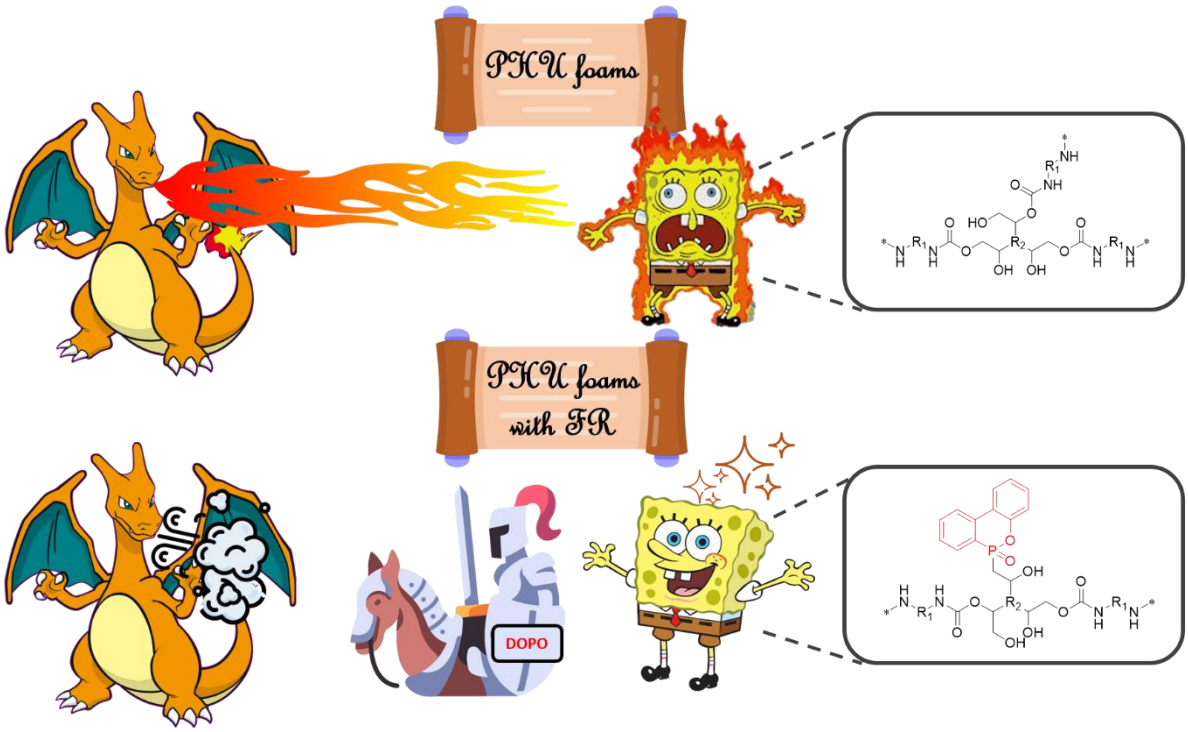

Abstract:
Polyurethane (PU) foams are widely used for many applications, however the use of toxic isocyanate monomers for their synthesis has recently led researchers to non-isocyanate PU foams. The most promising alternative is the aminolysis of cyclic carbonate which yields polyhydroxyurethanes (PHU). Nevertheless, the obtained foams suffer from significant flammability and require the introduction of flame retardants to improve their flame retardant properties. Hence, this article demonstrates the first synthesis of PHUs foams containing phosphorus-based flame retardants. The flame retardant were allowed to react with the monomers to prevent any leaching from the foams. Moreover, several structures of cyclic carbonates were analyzed in order to determine the influence of aromatic rings on both thermal stability and mechanical properties of foams by thermogravimetric analyses, differential scanning calorimetry and dynamic mechanical analyses. The flame retardant properties were studied with a cone calorimeter and pyrolysis combustion flow calorimeter. The best results were obtained by the foam containing 2 wt% of phosphorus and two aromatic rings in the cyclic

carbonate structure. Cone calorimeter analysis showed a total heat release of 13.1 KJ.g^{-1} versus 19.1 KJ.g^{-1} for the DOPO-free foam.

Keywords: Non-isocyanate polyurethane ; Foam ; Polyhydroxyurethane ; Flame retardant ; phosphorous ; DOPO.

1. Introduction

Polyurethane foams (PUFs) dominate the polymer foams market with a global production of 12Mt/y.[1,2] In 2020 the PUFs market was estimated around $38 billion and is expected to reach over $54 billion in 2025.[3] Moreover, due to their numerous properties such as light weight, thermal and sound insulation, high energy and shock absorption, PUFs are widely used in various applications.[4] However, due to their high carbon and hydrogen content, PUFs, as well as all organic polymers, exhibit flammability characteristics which results in the release of highly toxic fumes. Hence, some applications, such as bedding and furniture, automotive, building and construction require specific properties in order to protect consumers during utilization.[5,6,7] Therefore, flame retardants (FR) are incorporated to impart flame retardant properties and reduce the risk associated with their flammability. [8]

Generally, flame retardants are powders such as expandable graphite, alumina trihydrate, or brominated diphenyl oxide mixed directly into the PU formulation, prior to foaming.[9–12] Despite the simplicity of the method, this route suffers from many drawbacks such as modification of the mechanical and physical properties of obtained PUFs due to the presence of these solid additives. Hence, the flame retardant additives are not covalently bonded to the polymers and could migrate and modify the properties or leach out the foam which could lead to toxicity issues.[13] In addition, during prolonged use associated with aging, a loss of the flame retardant properties of the polymers is observed.[10] In recent decades, research has focused on reactive flame retardants which are generally halogen, phosphorus or nitrogen based.[8,14] Organohalogen flame retardants are very effective, but their use increases the amount of toxic and corrosive gases, such as CO and HBr, released during the combustion process.[14] Moreover, many halogen compounds are harmful to the environment and human health.[15] Hence, the European regulations have limited their use and their replacement has become a crucial issue.[16] Therefore, increasing attention has recently been paid to the development of halogen-free flame retardants. Phosphorus-based flame retardants are one of the most promising alternative to halogen flame retardants. Chen *et al.* have reported the synthesis of a phosphorus-containing triol, used as a reactive flame retardant to prepare PUFs.[17] Bhoyate *et al.* have synthetized a novel reactive flame retardant polyol based on phenylphosphonic acid grafted onto an epoxy in order to react with isocyanate to obtain PUFs.[18] Among these phosphorus flame retardants, 9,10-dihydro-9-oxa-10-phosphaphenanthrene 10-oxide (DOPO) have been developed and the interest of this compound comes from the ability to form a P-C bond by reaction with double bonds.[19] That is why several researches have focused on the synthesis of new DOPO-based flame retardants. Hence, Liu *et al.* have studied the influence of DOPO and its derivatives as flame retardants in polyurethane foams.[14] Xu *et al.* have also reported flame retardant properties of a DOPO-based polyol and its synergistic effect with expandable graphite in rigid polyurethane foams.[20] Zhao *et al.* have investigated the flame retardant properties of PUFs containing adducts of DOPO with a Schiff base.[21] More recently, Qian *et al*. have also studied the flame retardant properties of PUFs obtained by reaction between diisocyanates and a DOPO-based diol.[22] Nevertheless, in all those studies, PUFs are obtained by reaction between polyols and isocyanate monomers[23,24] and are blown by the reaction of isocyanate with moisture which produces carbon dioxide at room temperature.[25]

However, isocyanates are toxic substances, classified CMR (carcinogenic, mutagenic and reprotoxic) for the most common such as methylene diphenyl 4,4'-diisocyanate (MDI) and toluene diisocyanate (TDI). Hence, recent regulations are pushing to replace them and more sustainable alternatives are gaining increasing attention.[23,26] Among the recent advances in Non Isocyanate PolyUrethanes (NIPUs)[23,27–29] , polyhydroxyurethanes (PHU), resulting from the reaction of cyclic carbonate monomers and diamines, are one of the most promising routes.[30–35] Hence, PHU foams are also the most promising alternative to replace PUFs and until now, only a handful of works have been reported.[23,27,29,36–38] Only few carbonate monomers are commercially available and most of them are very expensive. Fortunately, they can be easily obtained by direct carbonation of oxiranes with carbon dioxide (CO_2). Thus, different epoxides have been selected in this work in order to study the influence of the structure on the properties of PHU foams thereof. Moreover, these monomers have been chosen to lead to rigid PHU foams which are generally used in building applications.
Furthermore, the synthesis of PHU foams containing reactive phosphorus-based flame retardants has never been reported. The general synthesis of phosphorus-carbonate used for the formulation of the foams are presented in Scheme 1. This study investigates the effectiveness of organophosphinate on the flame retardancy, mechanical and thermal properties of PHUs foams.

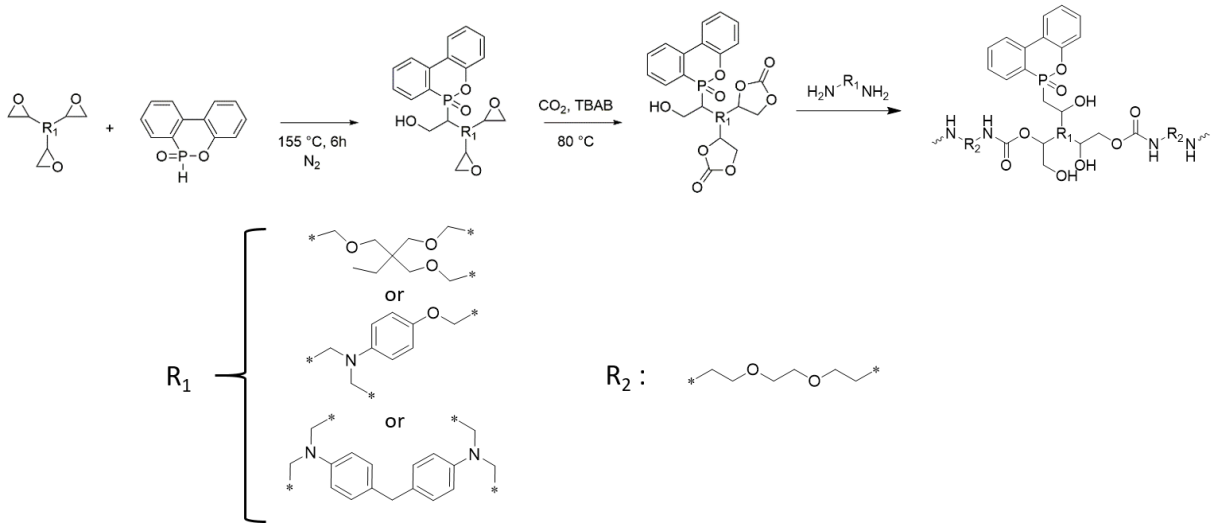

Scheme 1: general scheme of phosphorus flame retardant PHU foam

2. Experimental Part

1) Materials

9,10-dihydro-9-oxa-10-phosphaphenanthrene-10-oxide (DOPO) and 3,5-bis(trifluoromethyl)phenyl isothiocyanate (purity 98 %) were acquired from TCI. Poly(propylene glycol) diglycidyl ether (M_n = 640 $g.mol^{-1}$), Poly(methylhydrosiloxane) (PMHS, M_n = 2 080 $g.mol^{-1}$)[36], trimethylolpropane triglycidyl ether (TMPT), N,N-Diglycidyl-4-glycidyloxyaniline (DGGDA), 4,4'-Methylenebis(N,N-diglycidylaniline) (MBDA), tetrabutylammonium bromide (TBAB) (purity 99 %), 2,2-biphenol, phosphorus trichloride (PCl_3) and cyclohexylamine, were purchased from Sigma-Aldrich (Darmstadt Germany). Jeffamine® EDR-148 (2,2'-(ethylenedioxy)bis(ethylamine)) was kindly supply by Huntsman. CO_2 was acquired from Air Liquide. Ethyl acetate, dioxane, tetrahydrofuran and dichloromethane were purchased from VWR International S.A.S (Fontenay-sous-Bois, France). The NMR solvents used are $CDCl_3$ and DMSO from Eurisotop.

2) Characterizations

Nuclear Magnetic Resonance

NMR samples were prepared with $CDCl_3$ as solvent and the analyses were performed using a Bruker Avance 400 MHz spectrometer at 25 °C. The structure of monomers were determined by hydrogen nuclear magnetic resonance (^{1}H NMR), and phosphorus nuclear magnetic resonance (^{31}P NMR). External references were trimethylsilane (TMS) for ^{1}H and phosphoric acid (H_3PO_4) for ^{31}P NMR. Shifts were given in ppm.

Titration of the epoxy equivalent weight by ^{1}H NMR

The Epoxy Equivalent Weight (EEW) is the amount of epoxy monomer needed for one equivalent of reactive epoxy function. It was determined by ^{1}H NMR using an internal standard (benzophenone). Known masses of product and benzophenone were poured into a NMR tube and 550 µL of $CDCl_3$ were added. The EEW was determined using equation (1) by comparing the integration value of the signals assigned to the benzophenone protons (7.5-7.8 ppm) with the integration of the signals arising from epoxy protons (2.57 ppm).

$$EEW = \frac{\int PhCOPh \times H_{epoxy}}{\int epoxy \times H_{PhCOPh}} \times \frac{m_{epoxy}}{m_{PhCOPh}} \times M_{PhCOPh} \quad (1)$$

$\int_{PhCOPh}$: integration of the signal from benzophenone protons; $\int_{epoxy}$: integration of the signals from protons in α epoxy function; H_{epoxy}: number of protons in α of the epoxy function; H_{PhCOPh}: number of benzophenone protons; m_{epoxy}: epoxy mass; m_{PhCOPh}: benzophenone mass; M_{PhCOPh}: benzophenone molecular weight.

Titration of the amine equivalent weight of Jeffamine EDR-148 by ^{1}H NMR

The Amine Equivalent Weight (AEW) is the amount of Jeffamine needed for one equivalent of reactive amine function. It was determined by ^{1}H NMR using an internal standard (benzophenone). Known masses of product and benzophenone were poured into a NMR tube and 550 µL of $CDCl_3$ were added. The AEW was determined using equation (2) by comparing the integration value of the signals assigned to the benzophenone protons (7.5-7.8 ppm) with the integration of the signals arising from amine moiety protons (2.67 ppm).

$$AEW = \frac{\int PhCOPh \times H_{amine}}{\int amine \times H_{PhCOPh}} \times \frac{m_{amine}}{m_{PhCOPh}} \times M_{PhCOPh} \quad (2)$$

$\int_{PhCOPh}$: integration of the signal from benzophenone protons; $\int_{amine}$: integration of the signals from protons in α of the amine function; H_{amine}: number of protons in α of the amine function; H_{PhCOPh}: number of benzophenone protons; m_{amine}: amine mass; m_{PhCOPh}: benzophenone mass; M_{PhCOPh}: benzophenone molecular weight.

Titration of the carbonate equivalent weight by ^{1}H NMR

The Carbonate Equivalent Weight (CEW) is the amount of carbonate monomer needed for one equivalent of reactive cyclic carbonate function. It was determined by ^{1}H NMR using an internal standard (benzophenone). Known masses of product and benzophenone were poured into a NMR tube and 550 µL of $CDCl_3$.were added. The CEW was determined using equation (3) by comparing the integration value of the signals assigned to the benzophenone protons (7.5-7.8 ppm) with the integration of the signals arising from cyclic carbonate (4.85 ppm for TMPTC, 5.02 plus 5.14 for DDGDAC and 4.89 ppm for MBDAC).

$$CEW = \frac{\int PhCOPh \times H_{carbonate}}{\int carbonate \times H_{PhCOPh}} \times \frac{m_{carbonate}}{m_{PhCOPh}} \times M_{PhCOPh} \quad (3)$$

$\int_{PhCOPh}$: integration of the signal from benzophenone protons; $\int_{carbonate}$: integration of the signals from protons in α of the carbonate function; $H_{carbonate}$: number of protons in α of the carbonate function; H_{PhCOPh}: number of benzophenone protons; $m_{carbonate}$: product mass; m_{PhCOPh}: benzophenone mass; M_{PhCOPh}: benzophenone molecular weight.

Fourier Transform Infrared Spectroscopy

The Fourier transform infrared spectroscopy (FTIR) spectra were acquired on a Thermo Scientific Nicolet iS50 FT-IR equipped with an attenuated total reflectance cell (ATR). The data were analyzed using the software OMNIC Series 8.2 from Thermo Scientific.

Differential Scanning Calorimetry

Differential Scanning Calorimetry (DSC) analyses were carried out using a NETZSCH DSC200F3 calorimeter, which was calibrated using indium, n-octadecane n-octane, adamantane, biphenyl, tin, bismuth and zinc standards. Nitrogen was used as purge gas. Approximately 10 mg of sample were placed in a perforated aluminum pan and the thermal properties were recorded between -150 °C and 120 °C at 20 °C.min^{-1} to observe the glass transition temperature. The Tg values were measured on the second heating ramp to erase the thermal history of the polymer. All the reported temperatures are average values on three different experiments.

Dynamic Mechanical Analyses

Dynamic Mechanical Analyses (DMA) were carried out on Metravib DMA 25 with Dynatest 6.8 Software. Uniaxial stretching of foam samples (10x15x12 mm^3) was performed while heating at a rate of 3 °C.min^{-1} from -120 °C to 120 °C, keeping frequency at 1Hz.

The mechanical compression of the samples was measured at room temperature using 10x15x12 mm^3 foam samples in the creep mode with compression plate. The static maximum force used was fixed to 20 N with application time 60 s and maximum displacement of 30 % of strain and the time charging of 1 s. Then, the time of recovery of foams was measured during 60 s.

Hardness

Shore 0 hardness for foam was measured on a durometer Shore Hardness Tester HD0 100-1 from Sauter. Samples with 0.5 cm thickness were prepared for the measurement. An average of five measurements was performed.

Gel content

Three samples from the same material, of around 20 mg each, were separately immersed in THF for 24 h. The three samples were then rinsed and dried in a ventilated oven at 70 °C for 24 h. The gel content (GC) was calculated using equation (4), where m_2 is the mass of the dried material and m_1 is the initial mass. Reported gel content are average values of the three samples.

$$GC = \frac{m_2}{m_1} \times 100 \qquad (4)$$

Scanning electron microscopy

The morphology and the internal structure of the foams were analyzed using in parallel surface to the rise direction of NIPU foam by scanning electron microscopy (SEM). A FEI Quanta 200 FEG was used to obtained foam images. All the following results are obtained by average of measurement on 3 SEM images. The ratio A_h/A_c was obtained following the method of Fitzgerald et al.[39] It give information on the open-cell structure of the foams.

Some residues were analyzed using SEM-EDX (energy dispersive X-ray spectroscopy from Oxford INCA Energy system) in order to assess the fate of phosphorus (i.e. its presence in residue or its release in gaseous phase during burning). Residue from cone calorimeter may be highly heterogeneous and partially oxidized at the end of test. Therefore, it was preferred to analyze residues from PCFC (after pure anaerobic pyrolysis). 5 measurements were carried out in different parts of each residue to calculate the mean phosphorus content (in weight).

Thermogravimetric Analyses

Thermogravimetric analyses (TGA) of the cured foams were carried out to determine the thermal stability and were performed on a Netzsch TG 209F1 apparatus under 40 $mL.min^{-1}$ nitrogen flow. The protective gas used was nitrogen with a 20 $mL.min^{-1}$ flow. Approximately 10-12 mg of sample were placed in an alumina crucible and heated from room temperature to 800 °C with a 20 $°C.min^{-1}$ heating rate.

Pyrolysis combustion flow calorimeter analysis

Combustion properties of the foams was analyzed using a pyrolysis combustion flow calorimeter (PCFC). About 3-4 mg were placed in the pyrolyzer, undergoing an increase of temperature from 20 °C to 750 °C at a rate of 1 $°C.s^{-1}$ under a nitrogen flow. Pyrolytic gases were sent to a combustor heated at 900 °C under air flow (N_2/O_2 = 80/20). At this temperature and with 20 % of oxygen, combustion was considered to be complete. HRR was determined according to oxygen depletion (Huggett's relation) as cone calorimeter test. PCFC analyses correspond to anaerobic pyrolysis followed by high temperature oxidation of decomposition products (complete combustion)[40]. All samples were tested in triplicate.

Cone calorimeter test

Flammability was studied using a cone calorimeter in order to investigate the fire behavior of foams. The foams dimensions were 35X35 mm^2. All the samples exhibited a weight of 10 (±0.4) g. Consequently, their thickness changes depending on their density. The samples were placed at 2.5 cm below the conic heater and exposed to a 33 $kW.m^{-2}$ heat flux in well-ventilated conditions (air rate 24 $L.s^{-1}$) in the presence of a spark igniter to force the ignition. Heat release rate (HRR) was determined by oxygen depletion according to Huggett principle (1 kg of consumed oxygen corresponds to 13.1 MJ of heat released)[41]. The small non-standard dimensions of specimens have required a specific set-up. The samples were carefully embedded in rockwool (Figure 1) to avoid that heat flux was absorbed by the sample edges. No aluminum foil was used. When the foam presented a domed face, the flat surface was exposed to heat flux to ensure a homogeneous heat flux at the surface. During the test, the foam maintains its shape into the “rockwool mold” (except its thickness due to pyrolysis). This set-up ensures a good reproducibility of the test. The uncertainties are slightly higher than observed for standard specimens, especially because the surface area is only one eighth of the usual value. Nevertheless, the uncertainties are limited (typically ± 5 s for TTI and ± 50 $kW.m^{-2}$ for pHRR) comparing to the differences between foams. The HRR curve shape is clearly representative of the fire behavior of each foam. All samples were tested in duplicate.

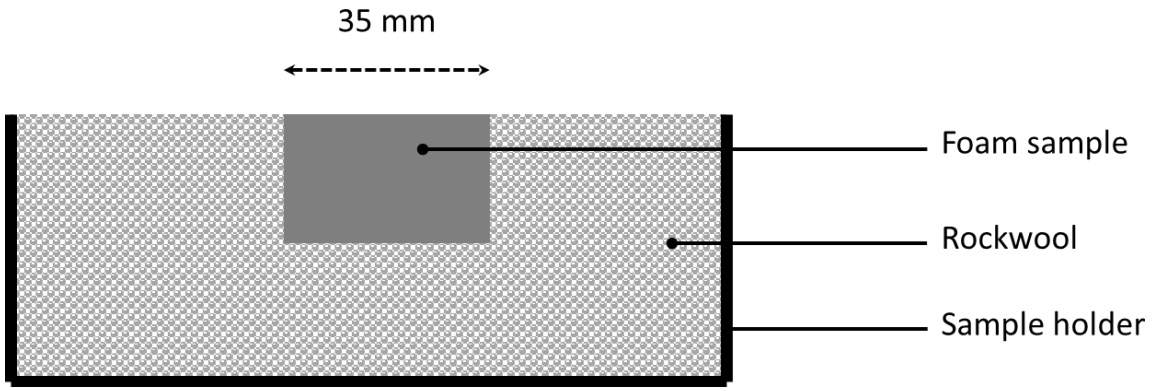

Figure 1: Foams set up for cone calorimeter

3) Synthesis

Synthesis of 1-(3,5-bis(trifluoromethyl)phenyl)-3-cyclohexylthiourea (thiourea)[37]

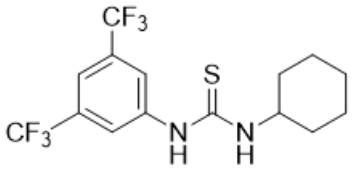

Figure 2: Thiourea structure

Thiourea, represented in Figure 2, was synthesized according to the literature procedure at room temperature, cyclohexylamine (14.63 g, 147.50 mmol) was added dropwise to a stirred solution of 3,5-bis(trifluoromethyl)phenyl isothiocyanate (40.00 g, 147.50 mmol) in THF (70 ml). After stirring for 4 h at room temperature, the solvent was evaporated. The white residue was recrystallized from chloroform to give thiourea as a white powder with 72% yield.
^{1}H NMR (400 MHz, $CDCl_3$, ppm): δ = 1.15 (d, 21H, CH_3), 3.33-3.95 (m, 25H, CH_2 and CH), 4.5 (m, 4H, CH_2-O(C=O)-O), 4.8 (t, 3H, CH-O(C=O)-O). (Figure SI 1)

Synthesis of 4,4'-(3,6,9,12,15,18,21-heptamethyl-2,5,8,11,14,17,20,23-octaoxatetracosane-1 ,24-diyl)bis(1,3-dioxolan-2-one) (PPO DC)

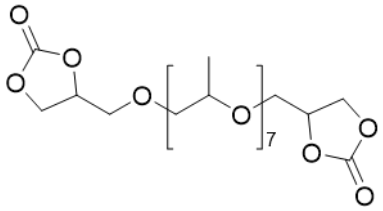

Figure 3: PPO DC structure

Poly(propylene glycol) diglycidyl ether (PPOGE 640; 300 g, 0.468 mol) and tetra-butylammonium bromide (TBAB; 4.53 g, 0.029 mmol) were solubilized in 200 mL of AcOEt and added to a 600 mL sealed reactor. The reaction was carried out at 80 °C under 20 bars of CO_2 for 120 h. The crude mixture was then washed with water and brine to remove TBAB. The organic layer was then dried with magnesium sulfate and under vacuum. The pure product, presented in Figure 3, was obtained as a yellowish viscous liquid with 93 % yield.^{1}H NMR (400 MHz, $CDCl_3$, ppm): δ = 1.15 (d, 21H, CH_3), 3.33-3.95 (m, 25H, CH_2 and CH of PPg unit), 4.5 (m, 4H, CH_2-O(C=O)-O), 4.8 (t, 3H, CH-O(C=O)-O). (Figure SI 2)

Synthesis of 4,4'-(((2-ethyl-2-(((2-oxo-1,3-dioxolan-4-yl)methoxy)methyl)propane-1,3-diyl)bis(oxy))bis(methylene))bis(1,3-dioxolan-2-one) (TMPTC)

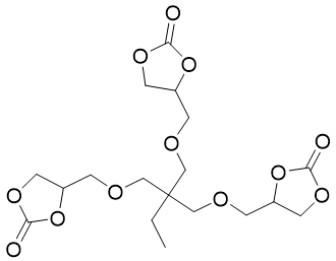

Figure 4: TMPTC structure

Trimethylolpropane triglycidyl ether (TMPT; 300 g, 0.99 mol, (Figure SI 3)) and tetrabutylammonium bromide (TBAB; 9.596 g, 0.029 mmol) were solubilized in 150 mL of AcOEt and added to a 600 mL sealed reactor. The reaction was carried out at 80 °C under 20 bars of CO_2 for 120 h. The crude mixture was then washed with water and brine to remove TBAB. The organic layer was then dried with magnesium sulfate and under vacuum. The pure product was obtained as a yellowish viscous liquid with 90 % yield. Figure 4 presented the TMPTC structure.

^{1}H NMR (400 MHz, $CDCl_3$, ppm): δ = 0.84 (t, 3H, CH_3), 1.41 (m, 2H, $\underline{CH_2}$-CH_3), 3.28-4.03 (m, 6H, Cq-$\underline{CH_2}$), 4.46 (m, 3H, $\underline{CH_2}$-O(C=O)-O), 4.49 (t, 3H, $\underline{CH_2}$-O(C=O)-O), 4.85 (m, 3H, $\underline{CH}$-O(C=O)-O). (Figure SI 4)

Synthesis of 6-(3-(2,2-bis((oxiran-2-ylmethoxy)methyl)butoxy)-2-hydroxypropyl) dibenzo [c,e][1,2]oxaphosphinine 6-oxide (TMPT-DOPO)

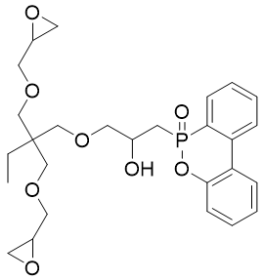

Figure 5: TMPT-DOPO structure

In a 500 mL three-necked round-bottom flask equipped with a condenser and a mechanical stirrer, 100 g (0.331 mol, 1 eq.) of TMPT and 71.44 g (0.331 mol, 1 eq.) of DOPO (Figures SI 5 and 6) were introduced and purged with N_2 during 30 min. Then, the reaction mixture was allowed to heat at 155 °C for 6h. At the end, the reaction was frozen and ground to obtain a white powder of TMPT-DOPO (Figure 5) with 96 % yield. The phosphorus ratio was 6 wt% in this flame retardant product and the EEW was 1.8.

^{1}H NMR (400 MHz, DMSO, ppm): δ = 0.81 (t, 3H, CH_3), 1.33 (m, 2H, $\underline{CH_2}$-CH_3), 2.22 (m, 2H, $\underline{CH_2}$-O-CH), 2.71 (t, 2H, $\underline{CH_2}$-O-CH), 3.07 (m, 2H, $\underline{CH}$-O-CH_2), 3.19-3.87 (m, 12H, CH_2 and CH-OH), 7.14-8.06 (m, 8H, Har). (Figure SI 7)

^{31}P NMR (400 MHz, DMSO, ppm): δ 35.4 ppm. (Figure SI 8)

HRMS (ESI+): calc. for [M + H^+] 519.21 g.mol^{-1}, found 519.21 g.mol^{-1}.

Synthesis of 4,4'-(((2-ethyl-2-((2-hydroxy-3-(6-oxidodibenzo[c,e][1,2]oxaphosphinin-6-yl)propoxy)methyl)propane-1,3-diyl)bis(oxy))bis(methylene))bis(1,3-dioxolan-2-one) (TMPTC-DOPO)

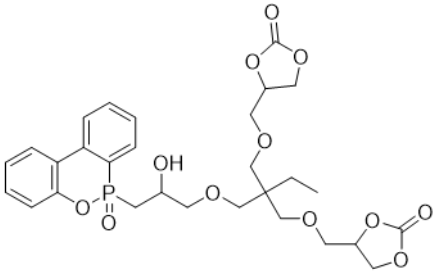

Figure 6: TMPTC-DOPO structure

TMPT-DOPO (200 g, 0.385 mol) and tetrabutylammonium bromide (3.730 g, 0.01 mmol) were solubilized in 200 mL of dichloromethane (DCM) and added to a 600 mL sealed reactor. The reaction was carried out at 80 °C under 20 bars of CO_2 for 120 h. The crude mixture was then washed with water and brine to remove TBAB. The organic layer was then dried with magnesium sulfate and under vacuum. The pure product, presented in Figure 6, was obtained as a yellowish viscous liquid with 80 % yield.

^{1}H NMR (400 MHz, DMSO, ppm): δ = 0.84 (t, 3H, CH_3), 1.41 (m, 2H, $\underline{CH_2}$-CH_3), 3.28-4.03 (m, 16H, $\underline{CH_2}$-O-$\underline{CH_2}$, $\underline{CH}$-OH and $\underline{CH_2}$-P), 4.46 (m, 2H, $\underline{CH_2}$-O-C(=O)-O), 4.49 (t, 2H, $\underline{CH_2}$-O-C(=O)-O), 4.85 (m, 2H, $\underline{CH}$-O-C(=O)-O), 6.87-8.21 (m, 8H, Har DOPO). (Figure SI 9)

^{31}P NMR (400 MHz, DMSO, ppm): δ 35.4 ppm. (Figure SI 10)

HRMS (ESI+): calc. for [M + H^+] 607.19 g.mol^{-1}, found 607.19 g.mol^{-1}.

Synthesis of 4,4'-(((4-((2-oxo-1,3-dioxolan-4-yl)methoxy)phenyl)azanediyl)bis(methylene)) bis(1,3-dioxolan-2-one) (DGGDAC)

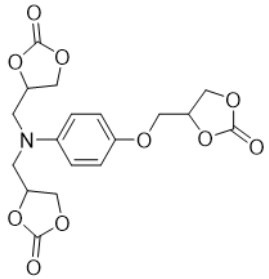

Figure 7: DGGDAC structure

N,N-Diglycidyl-4-glycidyloxyaniline (Figure SI 11) (100 g, 0.360 mol) and tetrabutylammonium bromide (3.487 g, 0.01 mmol) were solubilized in 100 mL of dichloromethane (DCM) and added to a 300 mL sealed reactor. The reaction was carried out at 80 °C under 20 bars of CO_2 for 120 h. The crude mixture was then washed with water and brine to remove TBAB. The organic layer was then dried with magnesium sulfate and under vacuum. The pure product (Figure 7) was obtained as a yellowish viscous liquid with 83 % yield.

^{1}H NMR (400 MHz, DMSO-d6, ppm): δ = 3.84 (m, 3H, $\underline{CH_2}$-N), 4.25 (m, 3H, $\underline{CH_2}$-O and $C\underline{H_2}$-O-C(=O)-O)-CH-CH_2-O, 4.43 (m, 1H, CH_2-O), 4.51 (m, 2H, $\underline{CH_2}$-C(=O)-O-CH-CH_2-N), 5.02 (m, 2H, $\underline{CH}$-O-C(=O)-O-CH-CH_2-N), 5.14 (m, 1H, O-CH_2-$\underline{CH}$-O-C(=O)-O), 6.79 (m, 4H, Har). (Figure SI 12)

Synthesis of 6-(1-hydroxy-3-((4-(oxiran-2-ylmethoxy)phenyl)(oxiran-2-ylmethyl)amino) propan-2-yl)dibenzo[c,e][1,2]oxaphosphinine 6-oxide (DGGDA-DOPO)

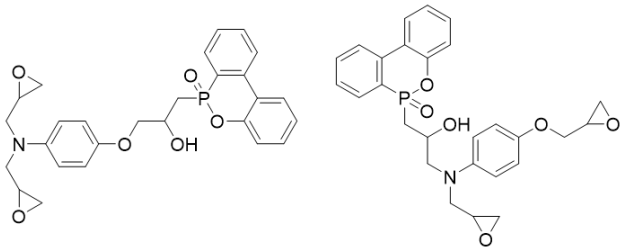

Figure 8: DGGDA-DOPO structure

In a 500 mL three-necked round-bottom flask equipped with a condenser and a mechanical stirrer, 100 g (0.361 mol, 1 eq.) of DGGDA and 77.89 g (0.361 mol, 1 eq.) of DOPO were introduced and purged with N_2 during 30 min. Then, the reaction mixture was allowed to heat at 155 °C for 6h. At the end, the reaction was frozen and ground to obtain a pale-yellow powder of DGGDA-DOPO (Figure 8) with 98 % yield. The phosphorus ratio was 6.3 wt% in this flame retardant product and the EEW was 2.

^{1}H NMR (400 MHz, DMSO, ppm): δ = 2.57 (m, 2H, $\underline{CH_2}$-O-CH), 2.74 (m, 2H, $\underline{CH_2}$-O-CH), 2.88 (t, 1H, $\underline{CH}$-O-CH_2), 3.15 (m, 2H, $\underline{CH}$-O-CH_2), 3.35 (m, 2H, CH_2-N), 3.67 (td, 2H, $\underline{CH_2}$-N), 3.91 (m, 1H, $\underline{CH}$-OH), 4.16 (dd, 1H, CH_2-P), 6.45-6.9 (m, 4H, Har), 7.09-8.20 (m, 8H, Har). (Figure SI 13)

^{31}P NMR (400 MHz, DMSO, ppm): δ 36.79 ppm. (Figure SI 14)

HRMS (ESI+): calc. for [M + H^+] 494.17 g.mol^{-1}, found 494.17 g.mol^{-1}.

Niklasson *et al.* have studied the impact of heteroatoms in the structure of phenyl glycidyl ether.[42] The study have demonstrated that heteroatoms such as oxygen and nitrogen have a similar reactivity. Those results allowed to conclude that there is a mixture of the two structures presented in Figure 7.

Synthesis of 4-((4-((3-hydroxy-2-(6-oxidodibenzo[c,e][1,2]oxaphosphinin-6-yl)propyl)((2-oxo-1,3-dioxolan-4-yl)methyl)amino)phenoxy)methyl)-1,3-dioxolan-2-one (DGGDAC-DOPO)

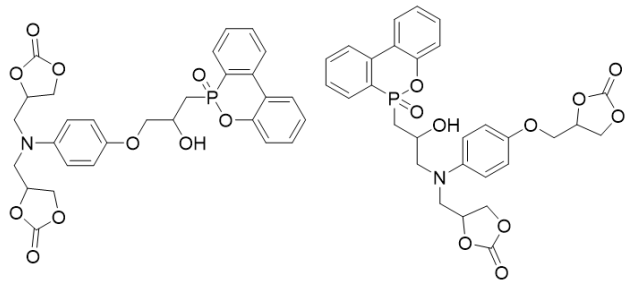

Figure 9: DGGDAC-DOPO structure

DGGDA-DOPO (200 g, 0.405 mol) and tetrabutylammonium bromide (3.919 g, 0.012 mmol) were solubilized in 200 mL of dichloromethane (DCM) and added to a 600 mL sealed reactor. The reaction was carried out at 80 °C under 20 bars of CO_2 for 120 h. The crude mixture was then washed with water and brine to remove TBAB. The organic layer was then dried with magnesium sulfate and under vacuum. The pure product, presented in Figure 9, was obtained as a yellowish viscous liquid with 78 % yield.

^{1}H NMR (400 MHz, DMSO, ppm): δ = 2.57-2.81 (m, 2H, $\underline{CH_2}$-P), 3.35-3.75 (m, 2H, $\underline{CH_2}$-N), 3.80-3.91 (m, 2H, $\underline{CH_2}$-O), 4.04-4.24 (m, 4H, $\underline{CH_2}$-O(C=O)-O), 4.38 (m, 1H, $\underline{CH_2}$-OH), 4.96-5.15 (m, 2H, $\underline{CH}$-O(C=O)-O), 6.45-6.93 (m, 4H, Har), 7.20-8.27 (m, 8H, Har). (Figure SI 15)

^{31}P NMR (400 MHz, DMSO, ppm): δ 36.79 ppm. (Figure SI 16)

HRMS (ESI+): calc. for [M + H^+] 582.15 g.mol^{-1}, found 582.15 g.mol^{-1}

Synthesis of 4,4',4'',4'''-(((methylenebis(4,1-phenylene))bis(azanetriyl))tetrakis(methylene))tetrakis(1,3-dioxolan-2-one) (MBDAC)

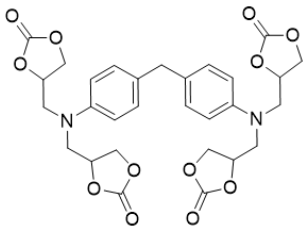

Figure 10: MBDAC structure

4,4'-Methylenebis(N,N-diglycidylaniline) (Figure SI 17) (100 g, 0.236 mol) and tetrabutylammonium bromide (2.29 g, 0.007 mmol) were solubilized in 150 mL of dichloromethane (DCM) and added to a 300 mL sealed reactor. The reaction was carried out at 80 °C under 20 bars of CO_2 for 120 h. The crude mixture was then washed with water and brine to remove TBAB. The organic layer was then dried with magnesium sulfate and under vacuum. The pure product (Figure 10) was obtained as a yellowish viscous liquid with 81 % yield.

^{1}H NMR (400 MHz, DMSO-d6, ppm): δ = 3.92 (m, 10H, $\underline{CH_2}$-Cq and CH_2-N), 4.27 (m, 4H, $\underline{CH_2}$-O(C=O)-O), 4.51 (m, 4H, $\underline{CH_2}$-O(C=O)-O), 4.89 (m, 4H, $\underline{CH}$-O(C=O)-O), 6.72 (m, 4H, Har), 7.10 (m, 4H, Har). (Figure SI 18)

Synthesis of 6-(3-((4-(4-(bis(oxiran-2-ylmethyl)amino)benzyl)phenyl)(oxiran-2-ylmethyl) amino)-2-hydroxypropyl)dibenzo[c,e][1,2]oxaphosphinine 6-oxide (MBDA-DOPO)

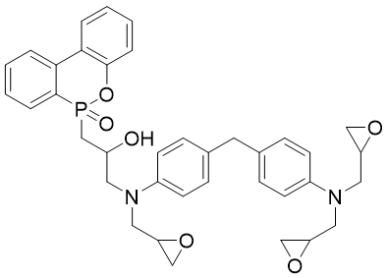

Figure 11: MBDA-DOPO structure

In a 500 mL three-necked round-bottom flask equipped with a condenser and a mechanical stirrer, 100 g (0.237 mol, 1 eq.) of MBDAC and 51.12 g (0.237 mol, 1 eq.) of DOPO were introduced and purged with N_2 during 30 min. Then, the reaction mixture was allowed to heat at 155 °C for 6h. At the end, the reaction was frozen and ground to obtain a pale orange powder of MBDA-DOPO (Figure 11) with 97 % yield. The phosphorus ratio was 5 wt% in this flame retardant product and the EEW was 3.

^{1}H NMR (400 MHz, DMSO, ppm): δ = 2.27 (m, 2H, $\underline{CH_2}$-P), 2.61 (m, 3H, $\underline{CH_2}$-O), 2.79 (m, 3H, $\underline{CH_2}$-O), 3.17 (m, 3H, $\underline{CH}$-O-CH_2), 3.45 (m, 4H, $\underline{CH_2}$-O-CH), 3.70 (dt, 4H, $\underline{CH_2}$-O-CH), 3.82 (s, 2H, $\underline{CH_2}$-$(ar)_2$, 6.76 (m, 4H, Har), 7.01 (m, 4H, Har), 7.09-8.20 (m, 8H, Har). (Figure SI 19)

^{31}P NMR (DMSO): δ 36.04 ppm. (Figure SI 20)

HRMS (ESI+): calc. for [M + H^+] 639.25 g.mol^{-1}, found 639.26 g.mol^{-1}.

Synthesis of 4,4'-(((4-(4-((2-hydroxy-3-(6-oxidodibenzo[c,e][1,2]oxaphosphinin-6-yl)propyl) ((2-oxo-1,3-dioxolan-4-yl)methyl)amino)benzyl)phenyl)azanediyl)bis(methylene))bis(1,3-dioxolan-2-one) (MBDAC-DOPO)

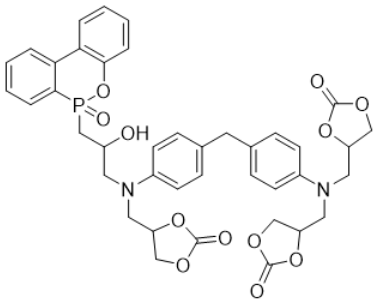

Figure 12: MBDAC-DOPO structure

MBDA-DOPO (200 g, 0.313 mol) and tetrabutylammonium bromide (3.03 g, 0.009 mmol) were solubilized in 200 mL of dichloromethane (DCM) and added to a 300 mL sealed reactor. The reaction was carried out at 80 °C under 20 bars of CO_2 for 120 h. The crude mixture was then washed with water and brine to remove TBAB. The organic layer was then dried with magnesium sulfate and under vacuum. The pure product, presented in Figure 12, was obtained as a yellowish viscous liquid with 78 % yield.

^{1}H NMR (400 MHz, DMSO, ppm): δ = 2.27 (m, 2H, $\underline{CH_2}$-P), 2.61 (m, 3H, $\underline{CH_2}$-O-C(=O)-O-CH), 2.79 (m, 3H, $\underline{CH_2}$-O-C(=O)-O-CH), 3.17 (m, 3H, $\underline{CH}$-O-C(=O)-CH_2), 3.45 (m, 4H, CH_2-N), 3.70 (dt, 4H, CH_2-N), 3.82 (s, 2H, $\underline{CH_2}$-$(ar)_2$), 4,1 (s, 1H, $\underline{CH}$-OH), 6.76 (m, 4H, Har), 7.01 (m, 4H, Har), 7.09-8.20 (m, 8H, Har). (Figure SI 21)

^{31}P NMR (400 MHz, DMSO, ppm): δ 36.04 ppm. (Figure SI 22)

HRMS (ESI+): calc. for [M + H^+] 771.22 g.mol^{-1}, found 771.23 g.mol^{-1}.

Table 1: Functionalities of carbonate monomers

	PPO DC	TMPTC	TMPTC-DOPO	DGGDAC	DGGDAC-DOPO	MBDAC	MBDAC-DOPO
Functionality	2.0	2.8	1.8	3.0	2.0	4.0	3.0

Foams formulations

All the foams were prepared with the same following procedure and exact masses were presented in supporting information (SI). The desire amounts of phosphorus-containing compounds and 0.024 mol of cyclic carbonates were introduced in vial with 0.85 mmol of the blowing agent (PMHS) and 5 wt% of the catalyst. The mixture was stirred with a SpeedMixer® for 10 minutes at 2 500 rpm. Then, 0.024 mol of the amine (EDR-148) were added and mixed for 30 sec at 2 500 rpm with to the SpeedMixer®. 10 g of the mixture were poured in a 35x35mm silicon mold and heated at 80 °C for 24 h and then 150 °C for 2 additional hours. All formulations were composed of one trifunctional or tetrafunctional carbonate and the same monomer modified with phosphorus group (foams with 1 and 2 wt%P) (0.7 molar eq.), PPO DC (0.3 molar eq) with EDR 148 (1 molar eq.), PMHS (0.05 eq.) and catalyst (0.03 eq.). In order to run fire tests each formulation was prepared three times in order to have two foams for cone calorimeter analysis and one for thermal and mechanical analysis. No additives was used to avoid an effect of the additives on the flame retardant properties. Indeed, usually the surfactant used are made from poly(siloxane-ether) which can influence the combustion?

Table 2: Foams formulation

Foams	Carbonate used	Wt% Phophorus
TMPTC	TMPTC	0%
DGGDMAC	DGGMDAC	0%

MBDAC	MBDAC	0%
TMPTC DOPO 1	TMPTC and TMPTC DOPO	1%
TMPTC DOPO 2	TMPTC and TMPTC DOPO	2%
DGGDMAC DOPO 1	DGGDMAC and DGGDMAC DOPO	1%
DGGDMAC DOPO 2	DGGDMAC and DGGDMAC DOPO	2%
MBDAC DOPO 1	MBDAC and MBDAC DOPO	1%
MBDAC DOPO 2	MBDAC and MBDAC DOPO	2%

3. Results and discussion

1) Synthesis of monomers and foams

Before the synthesis of monomers and PHU foams, a complete characterization of the raw materials has been carried out in order to determine their functionalities by ^{1}H NMR. The EEW calculated with equation (1) for trimethylolpropane triglycidyl ether (TMPT) was 2.8. The functionalization of one epoxy with 9,10-dihydro-9-oxa-10-phosphaphenanthrene-10-oxide (DOPO) had then led to a functionality of 1.8. However, to obtain a network, the functionality of all the monomers must be higher than 2. The TMPT was chosen as reference since it was already used by Cornille *et al.* for the synthesis of first PHU foams.[43] Two other epoxy compounds were also studied, N,N-diglycidyl-4-glycidyloxyaniline (DGGDMA) and 4,4'-methylenebis(N,N-diglycidylaniline) (MBDA). ^{1}H NMR and equation (1) allowed to determine their respective functionality of 3 and 4. DGGDMA and MBDA have been chosen for their structures that contain aromatic rings, which would provide rigidity and char formation during combustion. Different phosphorus contents were introduced in the foams, up to 2 wt% phosphorus. Indeed, even if 3wt% P was reported as an optimal percentage in a previous study[44], in the present formulation, such a content would lead to reducing the functionality of the epoxy monomers to less than 2, which would not allow crosslinking of the polymer. Therefore we have limited to 2 wt%. Regarding the Jeffamine EDR-148 (EDR-148), the titration confirmed the functionality of 2 amine functions. Indeed, the AEW is about 74 g/eq which is half of the molar mass of the amine.

Synthesis of epoxy-DOPO

The synthesis of epoxy-DOPO monomer is presented in Scheme 3. DOPO and epoxy monomers were added in stoichiometric ratio 1:1, in order to obtain only one DOPO per monomer while keeping at least two epoxy functions able to react during the second stage and the curing. The reaction was stirred at 155 °C for 6h. The synthesis was based on the nucleophilic attack of the P^{-} of the DOPO, obtained at high temperature, onto the epoxide group, leading to a P-C bond and a hydroxyl group. Moreover, the nucleophilic attack occurred on the less substituted carbon of the epoxide leading to the corresponding β-hydroxyphosphinates. The formation of P-C bond was determined by ^{31}P NMR. Indeed, in the ^{31}P NMR spectrum, the disappearance of the chemical shift of DOPO at 16 ppm and the appearance of the chemical shift at 36 ppm are characteristic of the formation of a P-C bond. The ^{1}H and ^{31}P NMR spectra are presented in supplemental information (SI figure 7, 8, 13, 14, 19, 20 for TMPT-DOPO, DGGDA-DOPO and MBDA-DOPO, respectively).

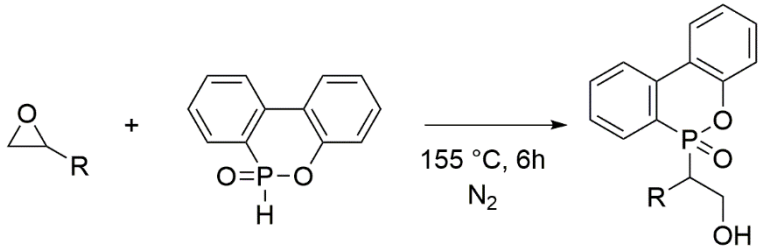

Scheme 2: Synthesis of phosphorus flame retardant epoxy monomer

The ^{1}H NMR was used to determine the EEW of epoxy monomers before and after reaction with DOPO. Hence, EEW of TMPT, DGGDA and MBDA were respectively 2.8, 3.0 and 4.0 before the reaction with DOPO. After reaction with DOPO, the EEW of TMPT-DOPO, DGGDA-DOPO and MBDA-DOPO were respectively 1.8, 2.0 and 3.0. Those results confirmed that only one epoxy group per molecule in average has reacted with DOPO.

Synthesis of carbonate monomers

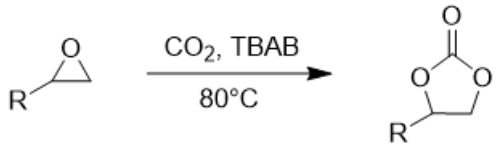

Scheme 3: Synthesis of carbonate monomer

The epoxy monomers obtained during the previous step were carbonated in order to obtain cyclic carbonates as presented in Scheme 4. Such reaction takes usually place in ethyl acetate, in pressurized reactor with 20 bars of CO_2, and with phase transfer catalyst (TBAB), .[43] This protocol was used with the TMPT. However, the other epoxy monomers required DCM in order to be well solubilized. After 120 h at 80 °C the reaction was stopped and the TBAB was removed by liquid-liquid extraction. The dried products were characterized by ^{1}H and ^{31}P NMR and FTIR (NMR: SI figure 4, 9, 10, 12, 15, 16, 18, 21, 22 and FTIR SI figure 23). The ^{1}H NMR analysis is used to determine the CEW of the molecules. These values are presented in Table 1. The CEW is linked to the number of carbonate functions by molecule. To obtain a thermoset, the functionality of one of the co-monomers has to be higher than 2. During the functionalization with DOPO, one epoxy was used, which decreases the functionality. Thus, before any foam synthesis the functionality of all the phosphorylated monomers was determined using the equation (3) and the values are presented in Table 1.

Formulations of foams

In this study nine different foam formulations have been studied. The foams were prepared at 80 °C by reaction between the different carbonates and EDR 148. The catalyst and the PMHS blowing agent have been chosen based on previous work in the literature.[43] A 1:1 ratio amine:(cyclic carbonate/cyclic carbonate-DOPO) was used for the formulations. For the formulation, all the solids were turned into a fine powder. First, the carbonate and the modified carbonate were added with PPO DC, the thiourea catalyst and the PMHS and mixed for 10 min with a SpeedMixer®. Then the amine was introduced and the formulation was mixed for an additional 30 s. The differences in structure of flame retardant foams were observed by scanning electron microscopy (SEM). Foam analyses were completed by the determination of the apparent density and also using DMA. Next, the crosslinking degree was determined by measurement of the swelling index and insoluble content. Finally, thermo-mechanical properties were studied by DSC and DMA. Shore 0 test for foams has been used to measure the hardness and conclude on the type of foams obtained. To determine the influence of phosphorus on the foam combustion behavior, cone calorimeter and PCFC were used.

2) Structural analysis

The FTIR analysis of all the synthetized foams showed the transformation of the C=O (1780 cm^{-1}) of the cyclic carbonate into urethane at 1690 cm^{-1} (Figure 13). Despite the cyclic carbonate conversion, a small peak at 1780 cm^{-1} of the cyclic carbonate can still be observed which shows uncompleted

conversion of the cyclic carbonate (Figure 13). Such results have been reported in literature, particularly when remaining functions are blocked in the polymer matrix.[45]

The gel contents have been measured in order to confirm the presence of a covalent network. For all the foams the results are higher than 80 % which confirms crosslinking (Table 3). The residual cyclic carbonate functions could also explain the non-quantitative gel content. The highest gel content with TMPTC can be explained by the higher miscibility of the monomers which leads to a better diffusion and therefore to a higher advancement of the reaction. Moreover, the formulations containing DGGDAC, MBDAC and the DOPO-modified monomers were dispersions of a solid in PPO 640. Thus it could induce a lower homogeneity of the dispersion and so tend to limit the advancement of the reaction.

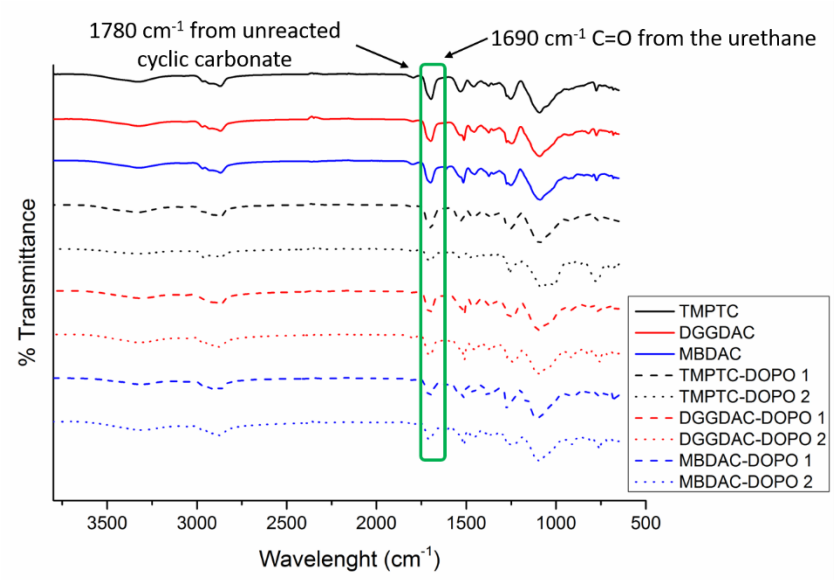

Figure 13: FTIR analyses of the different foams

Before SEM analysis, the foams were visually assessed in order to determine their homogeneity. From this analysis, on the first three foams a skin effect can be observed (Figure 14). The skin effect seems less important when the TMPTC-DOPO ratio is improved. It could be induced by the higher growth of the foam with TMPTC-DOPO 1 and TMPTC-DOPO 2. Nevertheless, the structure of the TMPTC and TMPTC-DOPO 1 foams are similar compared to the TMPTC-DOPO 2 foam. Thus it seems that the 2%wt P induced a new foam structure.

From Figure 14, 15 and 16, foams containing DOPO had higher expansion. It was visually confirmed when the foams were cut and the cell size was observed. The cell sizes increased with the %wtP. Such result is easily explained by the lower concentration of crosslinking nods when %wtP increases. Indeed, DOPO is grafted onto an epoxy function, which reduces the number of available epoxy groups for crosslinking and then the number of resulting crosslinking nods, allowing a higher foam growth. These results were confirmed by the foam density values (Table 2). The density of the foams was lowered with the increase of the %wt P. For example, the TMPTC-DOPO 2 foam had a reduced density of about 0.2 $g.cm^{-3}$ compared to the TMPTC-DOPO 1 foam and 0.4 $g.cm^{-3}$ compared to the phosphorus free TMPTC foam. All the foams followed the same trend (Table 2). Moreover, the foams with DGGDAC or MBDAC seem to have a higher expansion compared to the TMPTC foams which can be induced by the structure of the monomers and by the different CEW of each monomer. Indeed, a higher CEW means lower concentration of crosslinking nods and therefore a higher expansion. From these first results, a trend is observed. In order to have a precise idea of the foam structure and confirm the trend, SEM experiments were carried out.

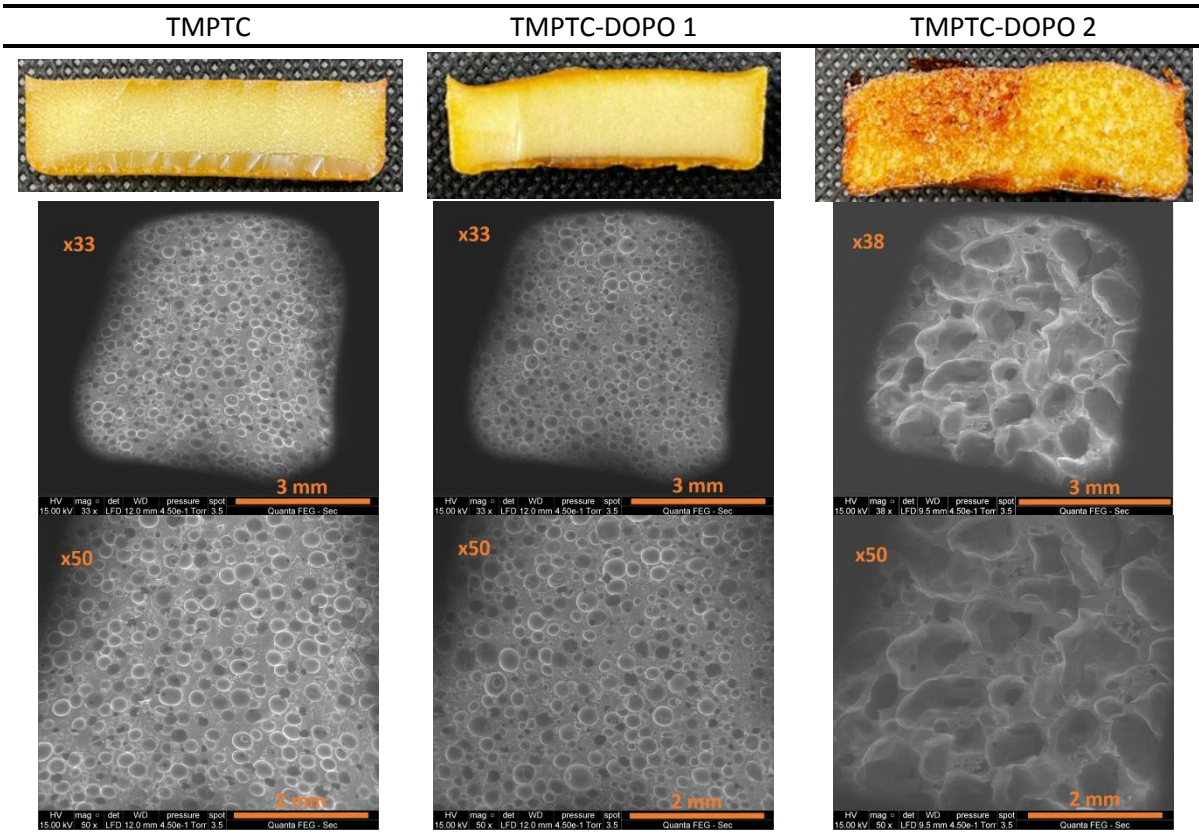

Figure 14: Images and SEM of foams containing TMPTC and 0, 1, 2 wt%P

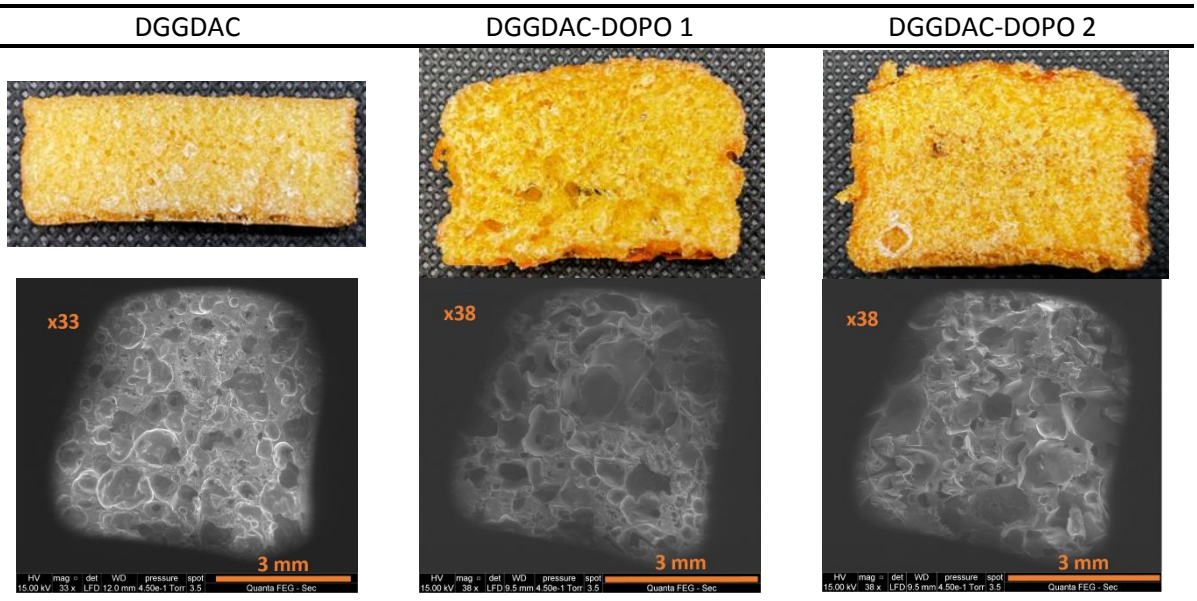

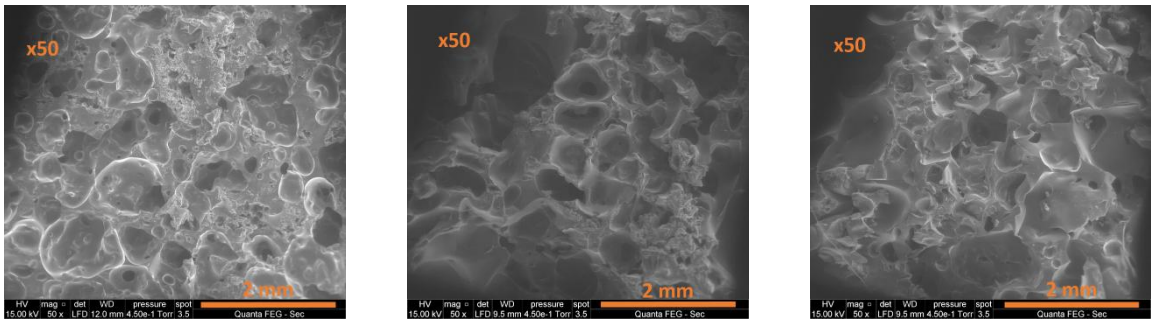

Figure 15: Images and SEM of foams containing DGGDAC and 0, 1, 2 wt%P

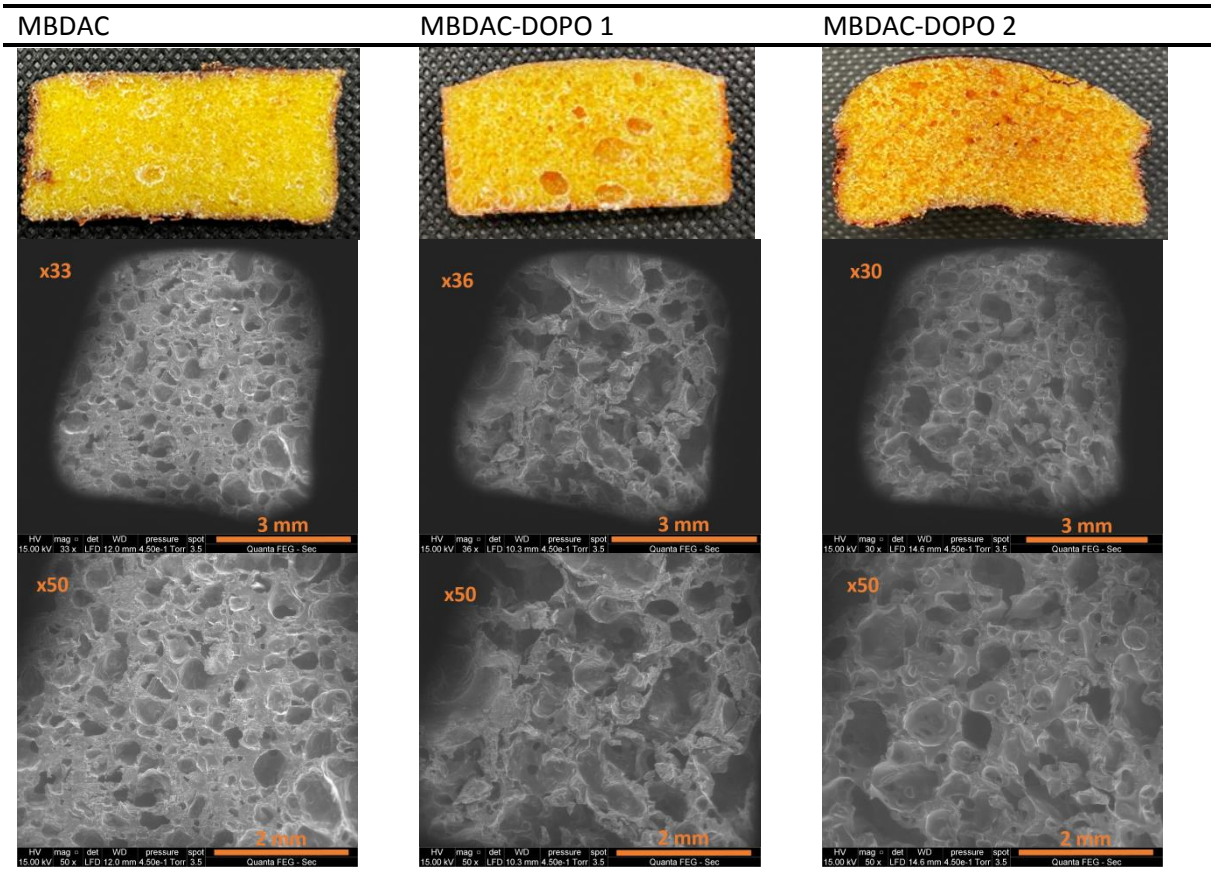

Figure 16: Images and SEM of foams containing MBDAC and 0, 1, 2 %wtP

SEM analyses were then carried out. The trend visually observed with higher expansion and lower density of the foam containing DOPO-modified monomers is confirmed by SEM analysis. For TMPTC, TMPTC-DOPO 1 and TMPTC DOPO 2 foams, the cell size increased with the phosphorus concentration. The foam with TMPTC had the smallest cells (Table 3) and the highest cell density (Ncell), around 1,375 cells.cm^{-3}. When the concentration of phosphorus increased, the cell sizes also increased, with respectively 290 ± 100 µm for 1 wt%P and 470 ± 200 µm for 2 wt%P. These results were consistent with the lower Ncell obtained. Hence, larger size cells occupy higher area in the SEM analysis. Thus, the NCell is lowered compared to small cell samples. Then, the ratio of holes area to cell area was measured (A_h/A_c). It helped to determine the interconnection of the pores.[38] When the ratio is close to 1 it corresponds to a foam with an open cell structure or interconnected cells. However, when the ratio is close to zero it means that the cells are not interconnected, which corresponds to a closed cell structure. The ratio (A_h/A_c) also increased with the cells size (Table 3). Thus, the higher cells size leads to open cell structure. It can be explained by a coalescence

phenomenon since these foams do not contain any additive that are generally used to obtain homogeneous foams and prevent coalescence and Ostwald ripening.[46]

The DGGDAC foam had average cell size about 590 ± 110 µm. Unlike TMPTC foams, cells size decreased with the increase of phosphorus concentration (Table 3). The great heterogeneity of phosphorus foams could explain this result. Indeed, larger pores are observed with SEM analysis but there are many small ones. Thus, a lower mean is obtained with a higher standard deviation. The heterogeneity is also confirmed by the Ncells of DGGDAC-DOPO 1 (455 ± 100 cells.cm-3) and DGGDAC-DOPO 2 (690 ± 140 cells.cm-3) foams which have important standard deviation. The MBDAC foam presented the same heterogeneous structure as the DGGDAC foams regarding the SEM pictures (Figure 15 and 16). MBDAC DOPO 1 and MBDAC DOPO 2 foams had lower density compared to MBDAC foam. For the 1 wt% P foam this is related to the higher cell size (0.42 ± 0.18 mm). The Ncell is lowered but the higher cell size lowered the density. MBDAC-DOPO 2 foam had lower cells size compared to the MBDAC DOPO 1 foam. Nevertheless, the lower density is explained by a higher Ncell. From these SEM pictures it can be concluded that the foams are relatively heterogeneous when the phosphorus concentration is improved.

Table 3: Structural analysis of the different foams

Foam	Cell size (mm)	ρ_a (g.cm^{-3})	Cell density (Ncell) (cells.cm^{-3})[a]	A_h/A_c
TMPTC	0.20 ± 0.05	0.832	1375 ± 100	0.15
TMPTC-DOPO 1	0.29 ± 0.10	0.693	860 ± 150	0.32
TMPTC-DOPO 2	0.47 ± 0.20	0.422	435 ± 40	0.35
DGGDAC	0.59 ± 0.11	0.579	575 ± 80	0.12
DGGDAC-DOPO 1	0.45 ± 0.25	0.343	455 ± 100	0.20
DGGDAC-DOPO 2	0.40 ± 0.20	0.323	690 ± 140	0.23
MBDAC	0.30 ± 0.14	0.483	930 ± 150	0.15
MBDA-DOPO 1	0.42 ± 0.18	0.411	700 ± 130	0.17
MBDA-DOPO 2	0.35 ± 0.16	0.301	1110 ± 70	0.19

[a]: Ncell= (nM/A)3/2ρs/ρp; the number in SEM image (n ,average on 3 images), magnification (M), surface area of the image (A, mm^2), sample density of solid (ρs) and foam density (ρp). The solid density was estimated at 1.068 ± 0.04 g.cm^{-3} on no-foamed samples.

3) DSC-DMA Thermo-mechanical analyses

First, DSC analyses were carried out to determine the glass transition temperatures (T_g) of the foams (Table 4). The TMPTC foam has a T_g around 3 °C while DGGDAC and MBDAC foams have a T_g of 5 °C and 8 °C, respectively (SI figure 32). The influence of the aromatic ring on the glass transition is well observed by DSC since the T_g value increases with the content of aromatic rings in the foam. Indeed, DGGDAC and MBDAC contain respectively one and two aromatic rings, conferring more rigidity to foams than TMPTC. The DOPO influence on the T_g has also been observed by DSC. According to the results (Table 4), when DOPO is included in the foam, the T_g is increased. The %wt P has also an influence, *e.g.* the MBDAC-DOPO 2 foam has a T_g about 39 °C while the MBDAC-DOPO 1 foam has a T_g around 23 °C (Figure SI 24). The same trend is observed for all the foams. A first explanation is the aromaticity of the DOPO which impart rigidity to the polymer (Figure SI 5). However these results are also influenced by the crosslinking nods concentration. Indeed, when the DOPO is grafted onto the monomers, their functionality is lowered, as is the concentration of crosslinking nods. However, depending on the monomer used, the influence of DOPO is not comparable. MBDAC DOPO monomer

has a functionality of about 3, so it acts as a curing agent, whereas TMPTC DOPO and DGGDAC DOPO, with a functionality of about 2, cannot lead to crosslinking. Thus the concentration of crosslinking nods counteracts the effect of DOPO for TMPTC and DGGDAC foams. Therefore MBDAC DOPO 2 foam has a higher T_g than DGGDAC DOPO 2 foam. The DGGDAC DOPO foam has a higher T_g than TMPTC DOPO foam due to the aromatic structure of the carbonate.
Then dynamic mechanical analyses were carried out on the foams in order to determine the α relaxation temperature corresponding to the transition from vitreous to elastic domains. The T_α also confirmed the DSC results (Figure SI 25 to 32). The monomers containing aromatic rings impart rigidity to the foams. Hence, the T_α of DGGDAC and MBDAC foam showed T_α of 38 °C and 33 °C respectively compared to 30 °C for TMPTC foam (Table 4, figure SI 25, 28, 30). Additionally, with the DOPO monomers, the T_α was further increased (figure SI 26, 27, 29, 31, 32), according to the trend observed by DSC and previously discussed. The 2 T_α TMPTC-DOPO 1 and TMPTC-DOPO foams were about 33 °C (*i.e.* close to the value of TMPTC). The difference is more important between DGGDAC and DGGDAC-DOPO 1 foams since T_α of DGGDAC-DOPO 1 foam reached 45 °C. The DGGDAC-DOPO 2 foam was not analyzed since the sample was too fragile and was broken during the DMA analysis. The T_α of phosphorus MBDAC foams also increased with the concentration of DOPO (Table 4).

Table 4: Mechanical analyses and thermal analyses

Foam	T_g (°C)[a]	T_α (°C)[b]	Shore test	Gel content (%)
TMPTC	3	31	42.4 ± 0.9	90
TMPTC-DOPO 1	9	33	43.2 ± 1.1	86
TMPTC-DOPO 2	20	33	67.9 ± 1.6	80
DGGDAC	5	38	63.3 ± 1.4	81
DGGDAC-DOPO 1	20	45	77.3 ± 3.1	80
DGGDAC-DOPO 2	22	-	51.6 ± 1.8	80
MBDAC	8	33	74.0 ± 0.9	82
MBDAC-DOPO 1	23	48	87.7 ± 2.9	81
MBDAC-DOPO 2	39	52	93.3 ± 0.8	80

[a]: T_g value determined by DSC; [b]: Tα value determined by DMA

The shore 0 hardness tests developed for foams have been carried out in order to measure the hardness of the foam. As for T_α, the hardness of the foam is strongly influenced by the chemical structure of carbonate monomer and by the concentration of DOPO which has an aromatic structure (Table 3). Hence, TMPTC foam had lower hardness than DGGDAC and MBDAC foams. The hardness also increased with the amount of DOPO introduced in the formulation. The DGGDAC foam had a lower hardness because the foam was brittle. As for DMA the foam broke during the analysis. To conclude the shore 0 test confirmed the DMA results. Such foams, excepted DGGDAC DOPO 2, could be used as rigid foam insulation between two walls for examples. However, for building application the flame retardant properties tested in the following part are crucial.

4) Thermal and flame retardant properties

Thermal and flame retardant properties were investigated and the results were reported in this part to highlight the influence of phosphorus and carbonate structure on the foam formulations.

The weight loss of the DOPO occurred in three steps, which can be noticed in the differential thermogravimetry (DTG) (Figure 17). The maximum weight loss (0.9%) of the first step was observed

at 95 °C. This weight loss may be caused by the evaporation of residual solvent. Then, the maximum weight loss of the second step (59%) was observed around 320 °C. At this temperature, the decomposition of the DOPO could occur from P-aryl bond whose cleavage requires less energy (272 $kJ.mol^{-1}$) than P-O bonds (360 $kJ.mol^{-1}$)[19]. The maximum weight loss of the third step (31%) was observed at 475 °C. This weight loss may be caused by the decomposition of DOPO which forms PO and PO_2 radicals[47]. Indeed, it is well known that DOPO decomposition produces PO radicals that mainly act in gaseous phase with little efficiency as char promoter[48].

The thermal properties of all the foams were analyzed by thermogravimetric analyses (TGA) under nitrogen flow. Figure 18 shows the thermograms of the foams with three different carbonates (TMPTC, DGGDAC, MBDAC) and various amounts of DOPO (0 wt%, 1 wt% and 2 wt% of phosphorus). Thermal parameters such as the decomposition temperature at 5 % weight loss ($T_{d,5wt\%}$), temperature at 50 % weight loss ($T_{d,50wt\%}$), and the residue yield at 750 °C, are summarized in Table 4. First, the temperature at 5 % weight loss slightly increased with the addition of DOPO-carbonates. Indeed, addition of DOPO-DGGDAC and DOPO-MBDAC improved the $T_{d,5wt\%}$ by 10 °C and 15 °C respectively. However, the addition of TMPTC-DOPO only increased the $T_{d,5wt\%}$ by 5 °C which is not significant. Regarding the temperature at 50 % weight loss ($T_{d,50wt\%}$), all the foams exhibited an equivalent thermal stability with temperatures between 345 °C and 351 °C. The residue yield of the foams depends on the carbonate structure and the amount of DOPO introduced. Indeed, for the reference samples, the highest residue yield was obtained with MBDAC (15.2 wt%) which contains two aromatic rings. The reference foam with DGGDAC, which contains only one aromatic ring, exhibited 13.3 wt% of residue at 750 °C. Finally, the TMPTC foam, which did not contain any aromatic ring, showed a residue yield of 10.8 wt% at 750 °C. Indeed, aromatics are well known to promote char formation. Moreover, the introduction of DOPO increased the foam residue yield to 19.8 wt% with the introduction of 1 wt% of phosphorus provided by DOPO in MBDAC foams. The residue yield increased by 2.2, 4.8 and 5.5 wt% for the foams with 2 wt%P TMPTC-DOPO, DGGDAC-DOPO, MBDAC-DOPO respectively, compared to the reference foam.

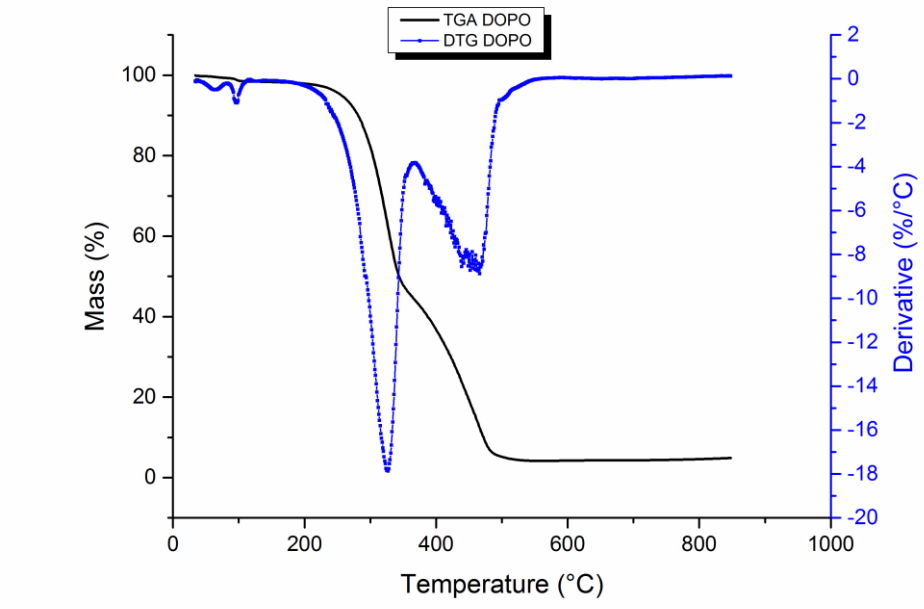

Figure 17: TGA and DTG curves of DOPO

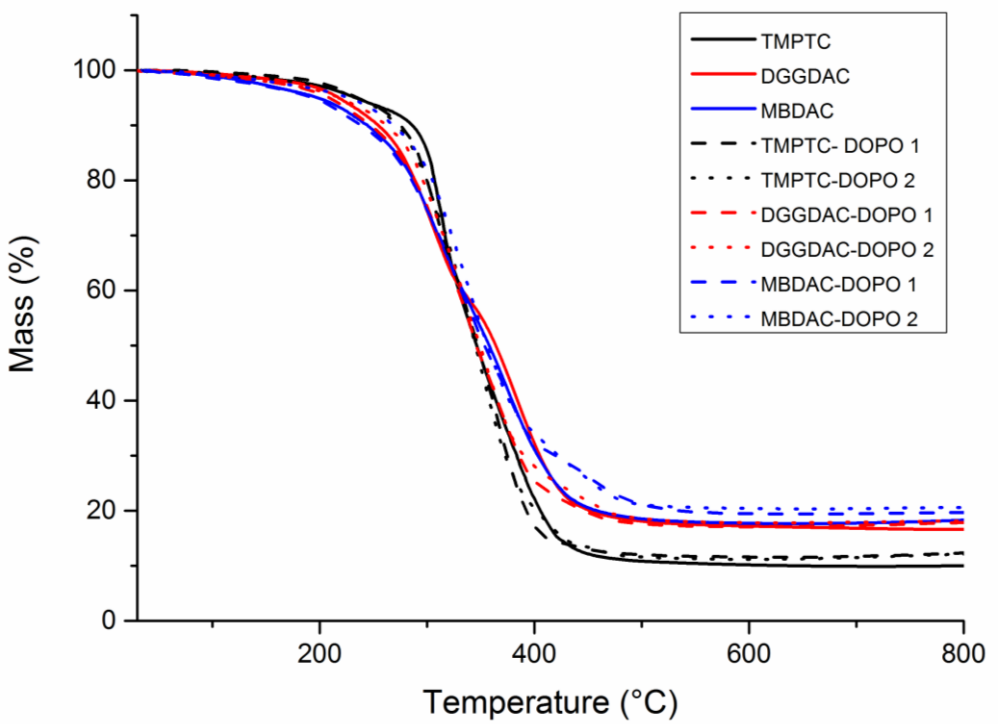

Figure 18: TGA curves of the foams

Table 4: Results of TGA analyses on foams

Samples	Td,5wt% (°C)	Td,50wt% (°C)	Td,max (°C)	Weight loss at Td,max (%)	Residue at 750°C (%)
TMPTC	220	346	346	75.9	10.2
DGGDAC	210	351	350	54.7	13.3
MBDAC	205	345	345	68.0	15.2
TMPTC-DOPO 1	225	347	346	77.4	12.6
DGGDAC-DOPO 1	220	346	342	71.9	18.0
MBDAC-DOPO 1	220	354	341	55.5	19.8
TMPTC-DOPO 2	226	345	345	79.1	12.4
DGGDAC-DOPO 2	225	349	355	60.1	18.1
MBDAC-DOPO 2	227	357	352	57.4	20.7

Pyrolysis combustion flow calorimeter analysis

Table 5 summarizes the data obtained from PCFC analyses. Under standard conditions, combustion is complete in PCFC test due to the combustion occurring in a combustion chamber at 900 °C in excess oxygen. Hence, the inhibitory effect of DOPO cannot be demonstrated in PCFC analysis.[49] This is why THR does not change significantly when incorporating higher DOPO contents. Only a slight increase may be expected whereas the contribution of DOPO to THR in PCFC was calculated at 27 kJ.g^{-1} (*i.e.* higher than the THR of the DOPO-free foams). Moreover, all the foams exhibited two peaks which means that their decomposition occurs in two apparent steps although the decomposition is

probably more complex with some small peaks or shoulders (Figure 19). A limited influence of DOPO is noticeable on the second pHRR which decreases with the increase of phosphorus content for MBDAC and DGGDAC foams. Indeed, for MBDAC foam, the second pHRR exhibited a value of 166 $W.g^{-1}$ whereas with the introduction of DOPO, the pHRR decreased from 159 $W.g^{-1}$ to 150 $W.g^{-1}$ with respectively 1 wt% and 2 wt% phosphorus. Moreover, Table 5 showed that the residue content increased with the amount of aromatic rings as well as with the amount of DOPO introduced in the foams but this effect is weak in comparison to other phosphorus groups as phosphonate.[49] Heat of complete combustion (Δh) is more or less constant while the charring is limited and the flame inhibition effect from DOPO is not effective.

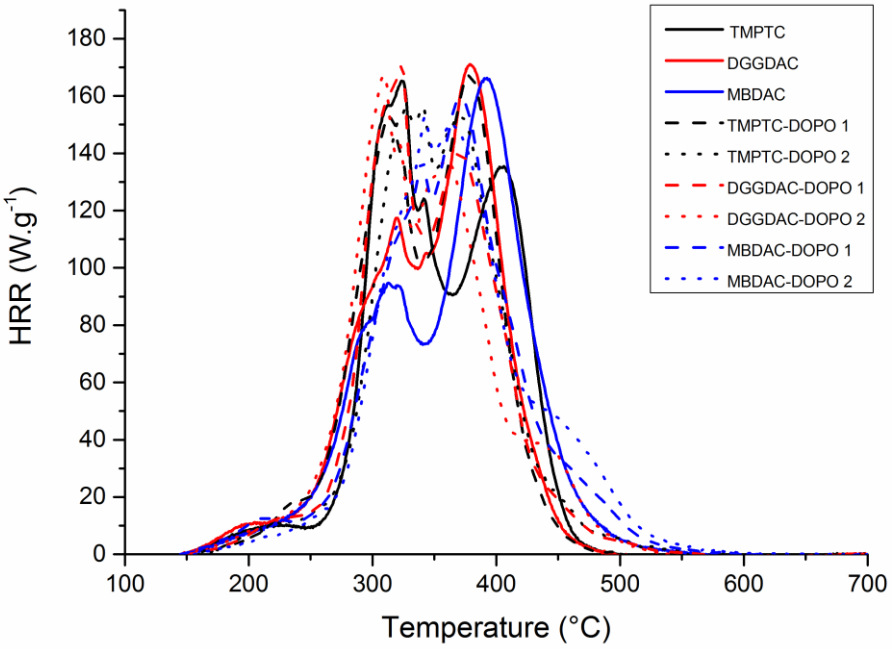

Figure 19: PCFC curves of the foams

Table 5: Results of PCFC analyses on foams

Samples	pHRR ($W.g^{-1}$)	T at pHRR (°C)	THR ($KJ.g^{-1}$)	Residue content (%)	Δh ($KJ.g^{-1}$)
TMPTC	165 and 135	324 and 406	19.8	1	20.1
DGGDAC	117 and 171	318 and 380	19.0	2	19.3
MBDAC	94 and 166	315 and 391	19.7	5	20.8
TMPTC-DOPO 1	152 and 167	316 and 377	19.6	1	19.9
DGGDAC-DOPO 1	171 and 140	324 and 370	19.2	4	19.9
MBDAC-DOPO 1	138 and 159	340 and 372	19.8	6	20.8
TMPTC-DOPO 2	151 and 153	326 and 370	19.3	4	20.2
DGGDAC-DOPO 2	167 and 138	309 and 358	19.5	5	20.6
MBDAC-DOPO 2	153 and 150	342 and 361	20.0	9	21.8

Cone calorimeter test

The cone calorimeter provides important information about the fire behavior of a material.[50] The main data are listed in Table 6 and HRR curves are shown in Figure 20. The fire behavior depends not only on the macromolecular network but also on the foam density which varies between 301 and 831 $kg.m^{-3}$ depending on the foam. Especially, a lower density corresponds to a limited heat transfer from the surface to the bulk resulting in a lower time-to-ignition (TTI). For a specific series, it can be observed that TTI slightly decreased with the density. Nevertheless, the influence of the network seems to be prevailing. The DGGDAC series showed the lowest TTI, almost two times less than for TMPTC series.

Peak of heat release rate is in the range 500-800 $kW.m^{-2}$. It was significantly higher for the TMPTC series while the DGGDAC and MBDAC series showed similar values. The shape of the HRR curve is more significant (Figures 20). In the case of the TMPTC series, the pHRR is followed by a plateau at a constant high value until a sharp decrease at extinction. This is indicative of a non-charring thermally thick behavior, *i.e.* the pyrolysis rate is constant and is not modified by some phenomena as the formation of a char layer able to limit progressively the heat transfer from the flame to the underlying material.[51] On the contrary, HRR curves for the two other series correspond to a charring thermally thick material, with a continuous decrease in HRR after reaching the pHRR. Therefore, the average pHRR (calculated during the flaming period, called avPHRR) is strongly reduced for both series. Indeed, avHRR is close to 600 $kW.m^{-2}$ for the series TMPTC but only in the range 223-380 $kW.m^{-2}$ for the series DGGDAC and MBDAC depending on the foam.
The aspect of residues after cone calorimeter tests confirms this interpretation. Indeed, there is no significant residue for the TMPTC series. On the contrary, for both DGGDAC and MBDAC series, a solid char layer is observed (Figure 22). This layer is formed few dozens of seconds after ignition. The formation of this layer corresponds to the stabilization of the HRR after a first phase of bubbling. This layer can thicken more and more during the test, and it is effective enough to limit the heat transfer despite a rather low final char content, especially for the MBDAC series, maybe due to thermo-oxidation at the end of the test. As explained above, it results in a continuous decrease of HRR until extinction. It should be noted that the PCFC results show that the carbonization content is still limited but higher for the DGGDAC and MBDAC series, probably due to the presence of aromatic groups.
It is noteworthy that DOPO has only a limited impact on weight loss rate (as seen in Figure 23 for the series MBDAC). The change in weight loss rate is probably impacted first by the density. DOPO did not change the shape of the HRR curves. Its influence is significant on the total heat release (THR) which decreased from around 19 $kJ.g^{-1}$ for DOPO-free foams to 13-15.4 $kJ.g^{-1}$ for 2 wt% P. Although charring was not improved by DOPO, these reduced THR values are fully attributed to the decrease in effective heat of combustion (EHC). DOPO is a poor char promoter but it acts mainly in gas phase as flame inhibitor (by trapping radicals). Indeed, DOPO did not lead to an increase in char content (Table 6). On the contrary, the combustion efficiency (calculated as the ratio between the effective heat of combustion and the heat of complete combustion measured in PCFC) is strongly reduced in presence of DOPO. DOPO-free foams exhibited an almost complete combustion. The combustion efficiency was close to 1 (or slightly higher, probably due to measurement uncertainties) but decreased to 0.71-0.84 and 0.62-0.82 for 1 and 2 wt% P respectively. A decrease in combustion efficiency means that oxidation of fuels in the flame is poorly effective, leading to a decrease in heat release. This phenomenon is generally accompanied by an increase in soot production, *i.e.* black smoke. Then

total smoke release (TSR) is also significantly increased with DOPO as observed in Figure 23. It is noteworthy that the decrease in combustion efficiency (*i.e.* the effect of DOPO) is more significant for the MBDAC series.

In order to assess the mode-of-action of phosphorus, some residues were analyzed by SEM-EDX. Residues from anaerobic pyrolysis in PCFC were preferred to avoid partial oxidation of char occurring at the end of cone calorimeter test. Residues from MBDAC-DOPO 2 and TMPTC-DOPO 2 contain around 2-3 wt% P (mean values 2.3 wt% and 2.5 wt% respectively). The residue from MBDAC-DOPO 1 contains a lower amount of phosphorus (1.9 wt%). On the contrary, the residue from DGGDAC-DOPO 2 contains a higher amount of phosphorus (3.5 wt%). According to the phosphorus content and the residue yield (given in Table 5), the fraction of phosphorus remaining in the residue can be calculated. In all cases, the major part of phosphorus is released in gas phase: only 11.4 wt%, 10 wt%, 5 wt% and 8.7 wt% of phosphorus remain in residue respectively for MBDAC-DOPO 1 and 2, TMPTC-DOPO 2 and DGGDAC 2. Even if these values must be considered as rough estimations, they are in agreement with the limited efficiency of DOPO as char promoter but also with the more significant decrease in combustion efficiency observed in cone calorimeter.

Table 6: Results of cone calorimeter analyses on foams

Samples	TTI (s)	pHRR ($KW.m^{-2}$)	avpHRR ($KW.m^{-2}$)	THR ($kJ.g^{-1}$)	Residue (wt%)	EHC ($MJ.Kg^{-1}$)	X	TSR (m^2/m^2)
TMPTC	45	806	606	19.4	0.6	19.5	0.97	1388
DGGDAC	24	547	382	18.9	8.2	20.8	1.08	2135
MBDAC	35	612	376	19.1	5.4	20.2	0.97	2917
TMPTC-DOPO 1	41	793	640	16.4	2.4	16.8	0.84	3627
DGGDAC-DOPO 1	25	514	224	15.3	6.2	16.3	0.82	3531
MBDAC-DOPO 1	32	678	332	14.4	3.2	14.9	0.71	4430
TMPTC-DOPO 2	39	726	594	15.4	5.1	16.3	0.81	5410
DGGDAC-DOPO 2	19	585	290	15.0	10.3	16.8	0.82	5597
MBDAC-DOPO 2	32	557	254	13.1	3.0	13.5	0.62	5682

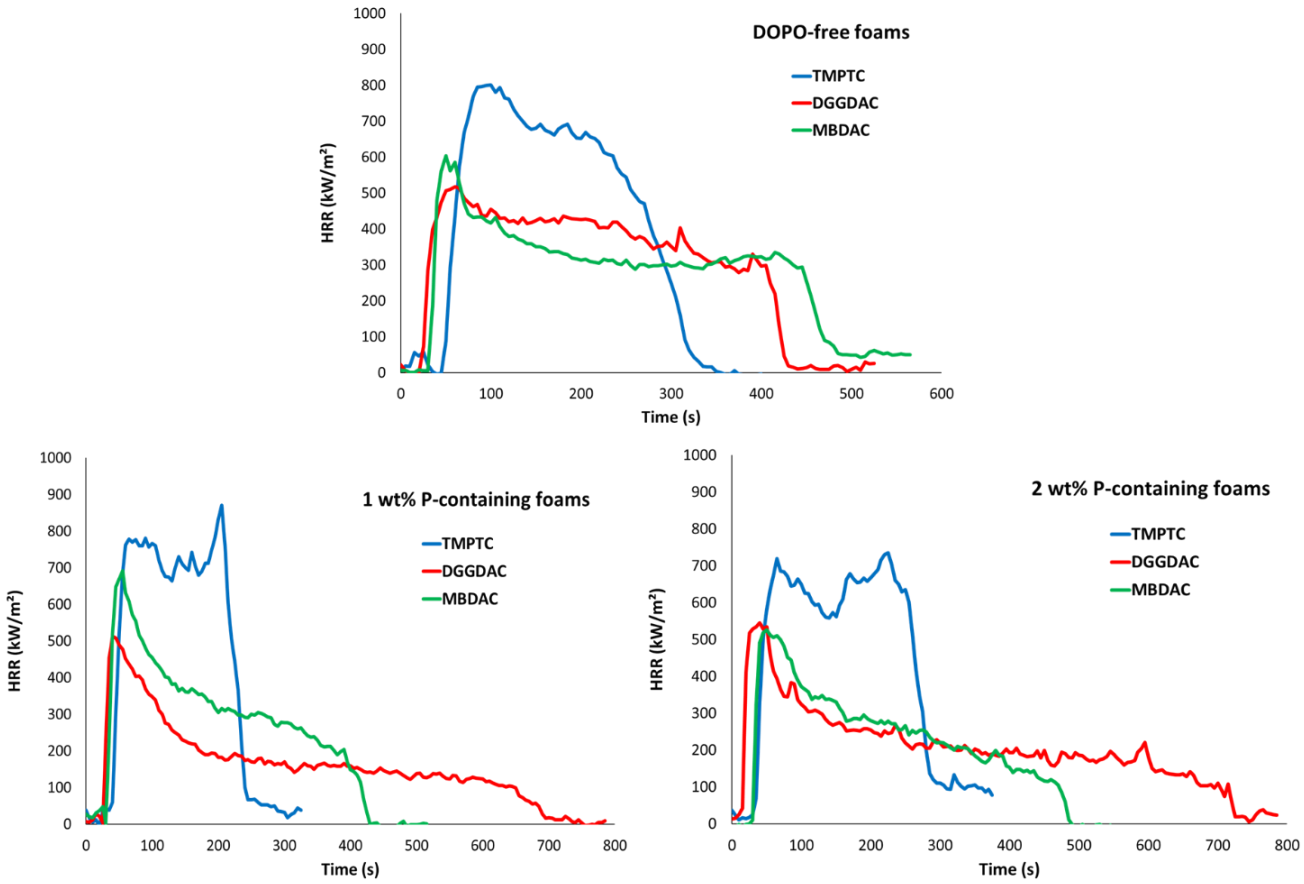

Figure 20: HRR curves of the foams in cone calorimeter (33 kW/m²)

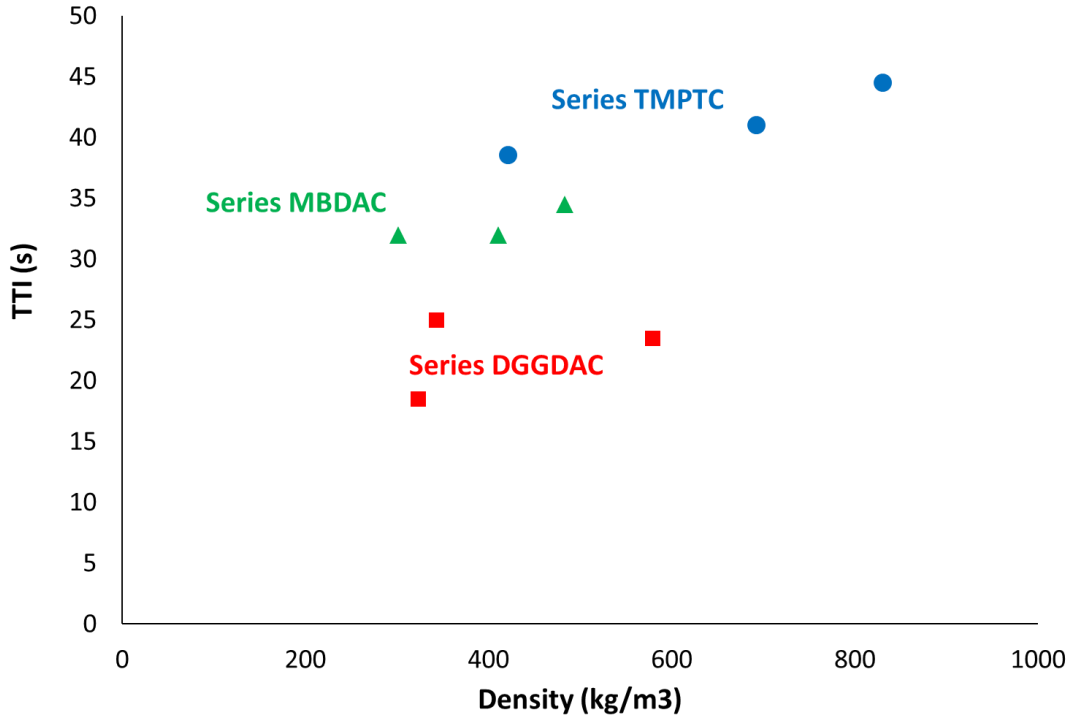

Figure 21: Time to ignition (TTI) versus density in cone calorimeter (33 kW/m²)

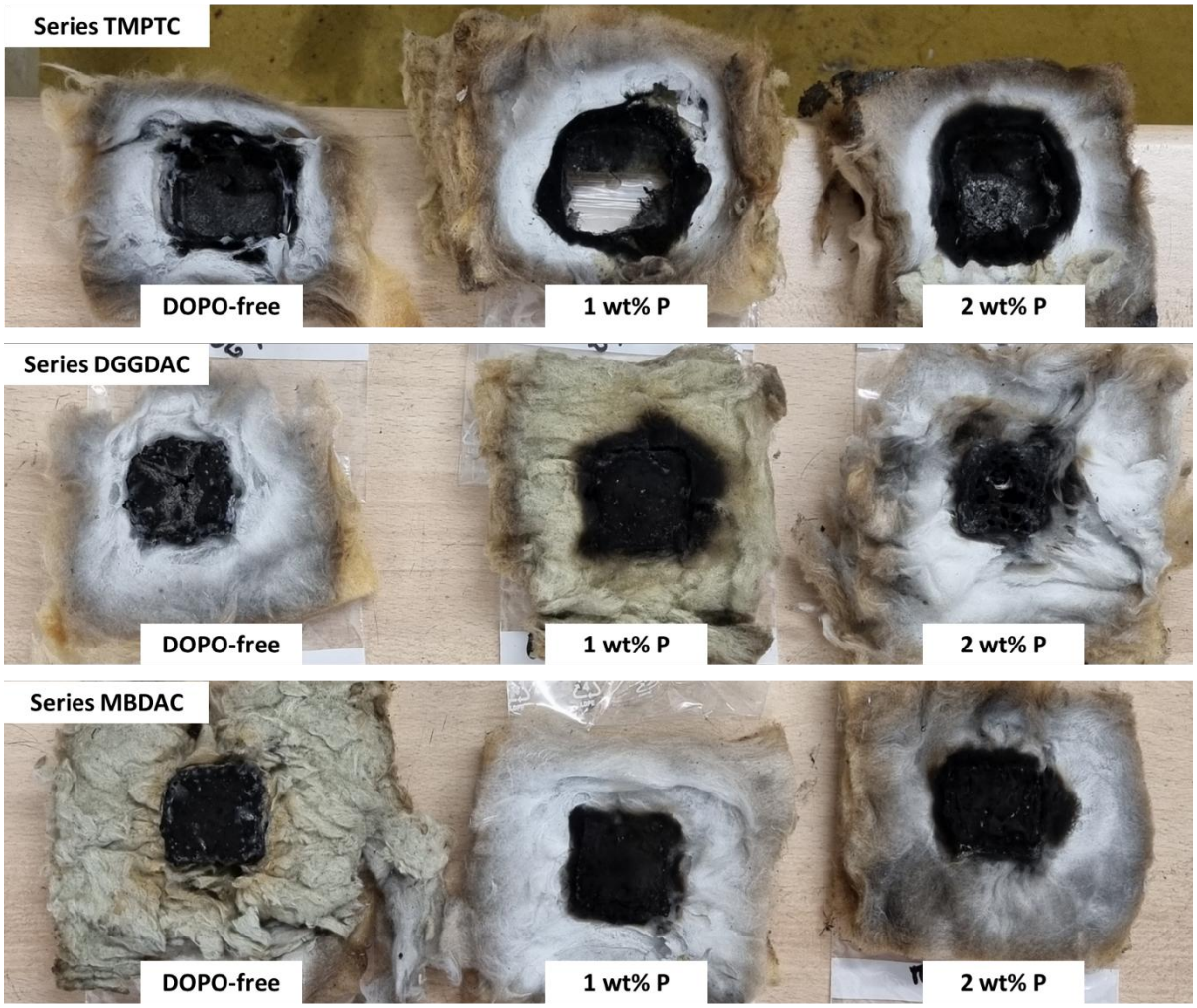

Figure 22: Residues of the foams after cone calorimeter test

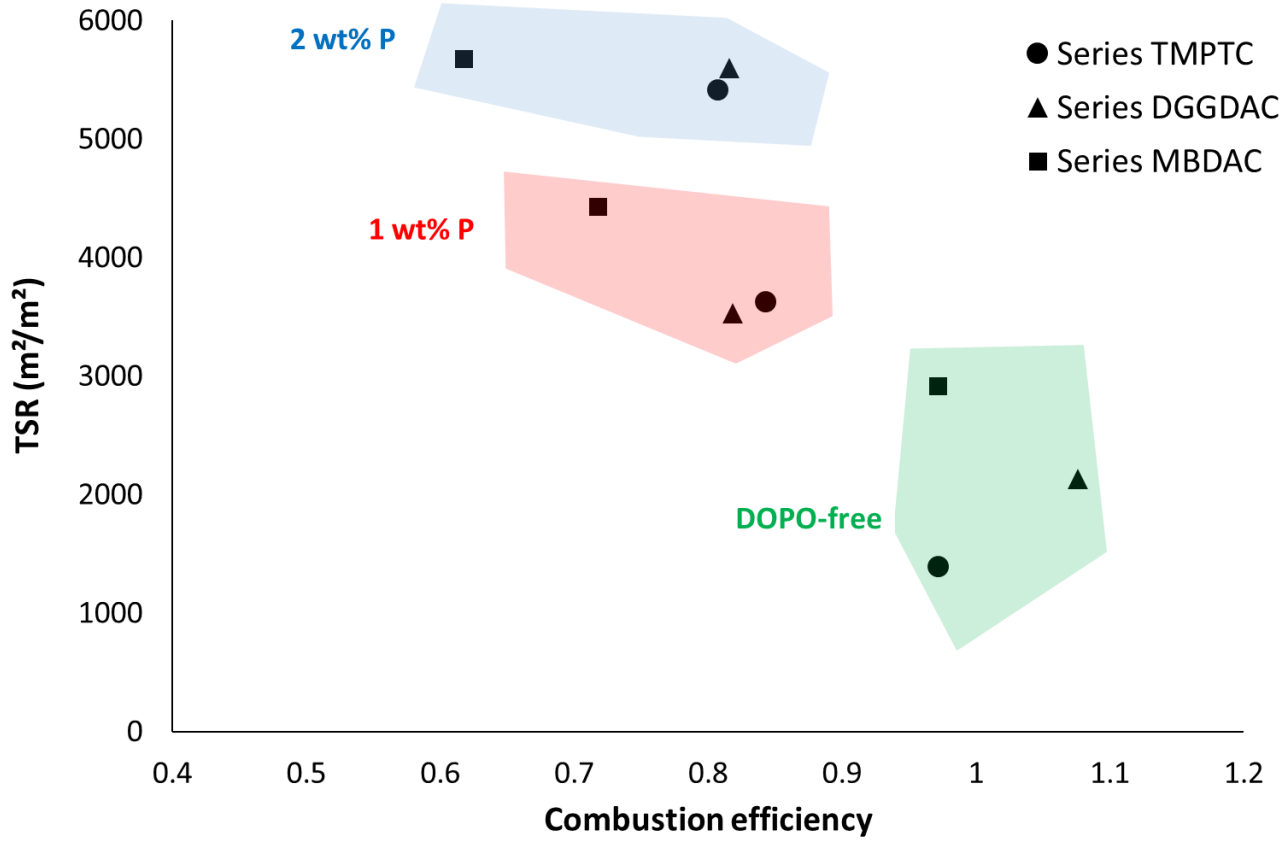

Figure 23: Total smoke release (TSR) versus combustion efficiency for all the foams in cone calorimeter

4. Conclusion

Novel DOPO-cyclic carbonates monomers have been successfully synthetized and used to obtain the first PHU foams with grafted flame retardant. Then, those foams have been characterized and the difference in structures was observed by SEM. The structures of cyclic carbonates impacted the physical and thermo-mechanical properties which have been analyzed by Shore 0 test, DMA, DSC. Indeed, the more aromatic rings there were incorporated into the foams, the more the rigidity increased. The fire behavior of those polymers has been analyzed by TGA, PCFC and cone calorimeter. All the DOPO-cyclic carbonate foams exhibited better thermal behavior than DOPO-free foams. Moreover, the aromatic rings of cyclic carbonates had a strong influence on the flame retardant properties. The residue was also favored by the number of aromatic rings in cyclic carbonates. Foams synthesized with DOPO-MBDAC have been shown to provide the best thermal stability and flame retardancy. Furthermore, the DOPO-MBDAC foams, containing 2 wt%P, exhibited a 31 % reduction in THR compared to the DOPO-free foam. These results are promising even if only flame retardancy of phosphinate was reported in this article. Phosphonate and phosphate flame retardants should also be studied because of their action in condensed phase which promotes char residue.

5. Acknowledgement

The authors would like to acknowledge Frédéric Fernandez from the MEA platform, Université de Montpellier, for the SEM experiments and sample preparation.

References:

(1) Polyurethane Production, Pricing and Market Demand https://www.plasticsinsight.com/resin-intelligence/resin-prices/polyurethane/ (accessed Jan 21, 2021).

(2) Coste, G.; Negrell, C.; Caillol, S. From Gas Release to Foam Synthesis, the Second Breath of Blowing Agents. *European Polymer Journal*. Elsevier Ltd November 5, 2020. https://doi.org/10.1016/j.eurpolymj.2020.110029.

(3) Polyurethane Foam Market by Type (Rigid Foam, Flexible Foam, Spray Foam), End-use Industry (Building & Construction, Bedding & Furniture, Automotive, Electronics, Footwear, Packaging, Others), and Region - Global Forecast to 2025 https://www.marketsandmarkets.com/Market-Reports/polyurethane-foams-market-1251.html?gclid=CjwKCAiA6aSABhApEiwA6Cbm_2xHisijomt3V8rNfWX6W1txxtbGAVQbmhiWku9iraGc2SdIia4urBoChPUQAvD_BwE (accessed Jan 21, 2021).

(4) Gama, N. V.; Ferreira, A.; Barros-Timmons, A. Polyurethane Foams: Past, Present, and Future. *Materials*. **2018**, 10, 1841-1876.

(5) Das, S.; Dave, M.; Wilkes, G. L. Characterization of Flexible Polyurethane Foams Based on Soybean-Based Polyols. *Journal of Applied Polymer Science*. **2009**, 299–308.

(6) Gama, N. V; Ferreira, A.; Barros-Timmons, A. Polyurethane Foams: Past, Present, and Future. *Materials*. **2018**, 1841–1876..

(7) Chen, X.; Li, J.; Xi, X.; Pizzi, A.; Zhou, X.; Fredon, E.; Du, G.; Gerardin, C. Condensed Tannin-Glucose-Based NIPU Bio-Foams of Improved Fire Retardancy. *Polym. Degrad. Stab.* **2020**, *175*, 109121.

(8) Dhaliwal, G. S.; Bajwa, D. S.; Bajwa, S. Fabrication and Testing of Soy‐Based Polyurethane Foam with Flame Retardant Properties. *Journal of Polymers and the Environment*. **2020**, 29, 1153-1161.

(9) Chen, M.-J.; Shao, Z.-B.; Wang, X.-L.; Chen, L.; Wang, Y.-Z. Halogen-Free Flame-Retardant Flexible Polyurethane Foam with a Novel Nitrogen−Phosphorus Flame Retardant. *Ind. Eng. Chem. Res.* **2012**, *51*, 9769–9776.

(10) Singh, H.; Jain, A. K. Ignition, Combustion, Toxicity, and Fire Retardancy of Polyurethane Foams: A Comprehensive Review. *J. Appl. Polym. Sci.* **2009**, *111*, 1115–1143.

(11) Thirumal, M.; Khastgir, D.; Singha, N. K.; Manjunath, B. S.; Naik, Y. P. Effect of Expandable Graphite on the Properties of Intumescent Flame-Retardant Polyurethane Foam. *J. Appl. Polym. Sci.* **2008**, *110* (5), 2586–2594..

(12) Bonsignore, P. V. Alumina Trihydrate as a Flame Retardant For Polyurethane Foams. *J. Cell. Plast.* **1981**, 220-225.

(13) Zhu, H.; Xu, S. Preparation of Flame-Retardant Rigid Polyurethane Foams by Combining Modified Melamine−Formaldehyde Resin and Phosphorus Flame Retardants. *ACS Omega* **2020**, *5*, 9658–9667.

(14) Liu, X.; Salmeia, K. A.; Rentsch, D.; Hao, J.; Gaan, S. Thermal Decomposition and Flammability of Rigid PU Foams Containing Some DOPO Derivatives and Other Phosphorus Compounds. *J. Anal. Appl. Pyrolysis* **2017**, *124*, 219–229.

(15) Van Der Veen, I.; De Boer, J. Phosphorus Flame Retardants: Properties, Production, Environmental Occurrence, Toxicity and Analysis. *Chemosphere* **2012**, *88*, 1119–1153.

(16) The European Parlament and the Council of the European Union. COMMISSION REGULATION (EC) No 552/2009. *Official Journal of the European Union*. 2009, 7–31.

(17) Chen, M.-J.; Chen, C.-R.; Tan, Y.; Huang, J.-Q.; Wang, X.-L.; Chen, L.; Wang, Y.-Z. Inherently Flame-Retardant Flexible Polyurethane Foam with Low Content of Phosphorus-Containing Cross-Linking Agent. *Ind. Eng. Chem. Res.* **2013**, *53*, 1160–1171.

(18) Bhoyate, S.; Ionescu, M.; Kahol, P. K.; Chen, J.; Mishra, S. R.; Gupta, R. K. Highly Flame-Retardant Polyurethane Foam Based on Reactive Phosphorus Polyol and Limonene-Based Polyol. *J. Appl. Polym. Sci.* **2018**, *135* (21), 46224.

(19) Wendels, S.; Chavez, T.; Bonnet, M.; Salmeia, K. A.; Gaan, S. Recent Developments in Organophosphorus Flame Retardants Containing P-C Bond and Their Applications. *Materials*.

2017, 10(7), 784.
(20) Xu, J.; Wu, Y.; Zhang, B.; Zhang, G. Synthesis and Synergistic Flame-Retardant Effects of Rigid Polyurethane Foams Used Reactive DOPO-Based Polyols Combination with Expandable Graphite. *J. Appl. Polym. Sci.* **2020**, 138, 50223.
(21) Zhao, Q.; Chen, C.; Fan, R.; Yuan, Y.; Xing, Y.; Ma, X. Halogen-Free Flame-Retardant Rigid Polyurethane Foam with a Nitrogen-Phosphorus Flame Retardant. *J. Fire Sci.* **2017**, *35* (2), 99–117.
(22) Qian, X.; Liu, Q.; Zhang, L.; Li, H.; Liu, J.; Yan, S. Synthesis of Reactive DOPO-Based Flame Retardant and Its Application in Rigid Polyisocyanurate-Polyurethane Foam. *Polym. Degrad. Stab.* **2022**, *197*, 109852.
(23) Xi, X.; Pizzi, A.; Gerardin, C.; Lei, H.; Chen, X.; Amirou, S. Preparation and Evaluation of Glucose Based Non-Isocyanate Polyurethane Self-Blowing Rigid Foams. *Polymers*. **2019**, 11, 1802.
(24) Frisch, K. C. History of Science and Technology of Polymeric Foams. *J. Macromol. Sci. Part A - Chem.* **1981**, *15* (6), 1089–1112.
(25) Ionescu, M. *Chemistry and Technology of Polyols for Polyurethanes , 2nd Edition Chemistry and Technology of Polyols for Polyurethanes , 2nd Edition*; **2016**; Vol. 2.
(26) 1907/2006/Ec. *Règlement (CE) No1907/2006 Du Parlement Européen et Du Conseil Du 18 Décembre 2006*; 2006.
(27) Clark, J. H.; Farmer, T. J.; Ingram, I. D. V.; Lie, Y.; North, M. Renewable Self-Blowing Non-Isocyanate Polyurethane Foams from Lysine and Sorbitol. *European J. Org. Chem.* **2018**, *2018* (31), 4265–4271.
(28) B. Grignard; J. M. Thomassin; S. Gennen; L. Poussard; L. Bonnaud; J. M. Raquez; P. Dubois; M. P. Tran; C. B. Park; C. Jerome; Detrembleur, C. CO2-Blown Microcellular Non-Isocyanate Polyurethane (NIPU) Foams: From Bio- and CO2-Sourced Monomers to Potentially Thermal Insulating Materials. *Green Chem.* **2015**, *18*, 2206–2215.
(29) Blattmann, H.; Lauth, M.; Mülhaupt, R. Flexible and Bio-Based Nonisocyanate Polyurethane (NIPU) Foams. *Macromol. Mater. Eng.* **2016**, *301* (8), 944–952.
(30) Steblyanko, A.; Choi, W.; Sanda, F.; Endo, T. Addition of Five-Membered Cyclic Carbonate with Amine. **2000**, *2380*, 2375–2380.
(31) Tomita, H.; Sanda, F.; Endo, T. Reactivity Comparison of Five- and Six-Membered Cyclic Carbonates with Amines: Basic Evaluation for Synthesis of Poly(Hydroxyurethane). *J. Polym. Sci. Part A Polym. Chem.* **2001**, *39* (1), 162–168.
(32) Kihara, N.; Endo, T. Synthesis and Properties of Poly(Hydroxyurethane)S. *J. Polym. Sci. Part A Polym. Chem.* **1993**, *31* (11), 2765–2773.
(33) Steblyanko, A.; Choi, W.; Sanda, F.; Endo, T. Addition of Five-Membered Cyclic Carbonate with Amine and Its Application to Polymer Synthesis. *J. Polym. Sci. Part A Polym. Chem.* **2000**, *38* (13), 2375–2380.
(34) Kihara, N.; Kushida, Y.; Endo, T. Optically Active Poly(Hydroxyurethane)s Derived from Cyclic Carbonate and L-Lysine Derivatives. *J. Polym. Sci. Part A Polym. Chem.* **1996**, *34* (11), 2173–2179.
(35) Benyahya, S.; Boutevin, B.; Caillol, S.; Lapinte, V.; Habas, J. P. Optimization of the Synthesis of Polyhydroxyurethanes Using Dynamic Rheometry. *Polym. Int.* **2012**, *61* (6), 918–925.
(36) Cornille, A.; Dworakowska, S.; Bogdal, D.; Boutevin, B.; Caillol, S. A New Way of Creating Cellular Polyurethane Materials: NIPU Foams. *Eur. Polym. J.* **2015**, *66*, 129–138.
(37) Cornille, A.; Guillet, C.; Benyahya, S.; Negrell, C.; Boutevin, B.; Caillol, S. Room Temperature Flexible Isocyanate-Free Polyurethane Foams. *Eur. Polym. J.* **2016**, *84*, 873–888.
(38) Monie, F.; Grignard, B.; Thomassin, J. M.; Mereau, R.; Tassaing, T.; Jerome, C.; Detrembleur, C. Chemo- and Regioselective Additions of Nucleophiles to Cyclic Carbonates for the Preparation of Self-Blowing Non-Isocyanate Polyurethane Foams. *Angew. Chemie - Int. Ed.* **2020**, *59* (39), 17033–17041.
(39) Fitzgerald, C.; Lyn, I.; Mills, N. J. Airflow through Polyurethane Foams with Near-Circular Cell-Face Holes. *J. Cell. Plast.* **2004**, *40* (2), 89–110.

(40) Laoutid, F.; Bonnaud, L.; Alexandre, M.; Lopez-Cuesta, J. M.; Dubois, P. New Prospects in Flame Retardant Polymer Materials: From Fundamentals to Nanocomposites. Materials Science and Engineering R: Reports. **2009**, 100–125.
(41) Huggett, C. Estimation of Rate of Heat Release by Means of Oxygen Consumption Measurements. *Fire Mater.* **1980**, *4* (2), 61–65.
(42) Niklasson, I. B.; Delaine, T.; Luthman, K.; Karlberg, A. T. Impact of a Heteroatom in a Structure-Activity Relationship Study on Analogues of Phenyl Glycidyl Ether (PGE) from Epoxy Resin Systems. *Chem. Res. Toxicol.* **2011**, *24* (4), 542–548.
(43) Cornille, A.; Dworakowska, S.; Bogdal, D.; Boutevin, B.; Caillol, S. A New Way of Creating Cellular Polyurethane Materials: NIPU Foams. *Eur. Polym. J.* **2015**, *66*, 129–138.
(44) Ménard, R.; Negrell, C.; Fache, M.; Ferry, L.; Sonnier, R.; David, G. From a Bio-Based Phosphorus-Containing Epoxy Monomer to Fully Bio-Based Flame-Retardant Thermosets. *RSC Advances*. 2015, pp 70856–70867. https://doi.org/10.1039/c5ra12859e.
(45) Blain, M.; Cornille, A.; Boutevin, B.; Auvergne, R.; Benazet, D.; Andrioletti, B.; Caillol, S. Hydrogen Bonds Prevent Obtaining High Molar Mass PHUs. *J. Appl. Polym. Sci.* **2017**, No. 44958, 1–13.
(46) Peyrton, J.; Avérous, L. Structure-Properties Relationships of Cellular Materials from Biobased Polyurethane Foams. *Mater. Sci. Eng. R Reports* **2021**, *145* (March).
(47) Salmeia, K. A.; Gaan, S. An Overview of Some Recent Advances in DOPO-Derivatives: Chemistry and Flame Retardant Applications. *Polym. Degrad. Stab.* **2015**, *113*, 119–134. https://doi.org/10.1016/j.polymdegradstab.2014.12.014.
(48) Negrell, C.; Frénéhard, O.; Sonnier, R.; Dumazert, L.; Briffaud, T.; Flat, J. J. Self-Extinguishing Bio-Based Polyamides. *Polym. Degrad. Stab.* **2016**, *134*, 10–18.
(49) Sonnier, R.; Otazaghine, B.; Vagner, C.; Bier, F.; Six, J. L.; Durand, A.; Vahabi, H. Exploring the Contribution of Two Phosphorus-Based Groups to Polymer Flammability via Pyrolysis-Combustion Flow Calorimetry. *Materials*. **2019,** 12, 2961.
(50) McNally, T.; Pötschke, P.; Halley, P.; Murphy, M.; Martin, D.; Bell, S. E. J.; Brennan, G. P.; Bein, D.; Lemoine, P.; Quinn, J. P. Polyethylene Multiwalled Carbon Nanotube Composites. *Polymer*. **2005**, 8222–8232.
(51) Schartel, B.; Hull, T. R. Development of Fire-Retarded Materials - Interpretation of Cone Calorimeter Data. *Fire Mater.* **2007**, *31* (5), 327–354.